minerals

MDPI

Article

$^{40}Ar/^{39}Ar$ Geochronology of Magmatic-Steam Alunite from Alunite Ridge and Deer Trail Mountain, Marysvale Volcanic Field, Utah: Timing and Duration of Miocene Hydrothermal Activity Associated with Concealed Intrusions

Cameron M. Mercer [1,*], Michael A. Cosca [1], Albert H. Hofstra [1], Wayne R. Premo [2], Robert O. Rye [3,†] and Gary P. Landis [3,†]

[1] U.S. Geological Survey, Geology, Geophysics, and Geochemistry Science Center, Denver, CO 80225, USA
[2] U.S. Geological Survey, Geosciences and Environmental Change Science Center, Denver, CO 80225, USA
[3] U.S. Geological Survey, Denver, CO 80225, USA
* Correspondence: cmmercer@usgs.gov
† Retired.

Abstract: Porphyry and epithermal deposits are important sources of base and precious metals. Most actively mined deposits have been exhumed such that ore bodies are relatively close to the surface and are therefore locatable and economic to extract. Identifying and characterizing concealed deposits, particularly more deeply buried porphyry deposits, represents a far greater challenge for mineral exploration, and will become progressively more important as near-surface resources are gradually exhausted over time. We report high-precision $^{40}Ar/^{39}Ar$ dates for coarsely crystalline alunite that precipitated from magmatic steam in open fractures in Oligocene dacitic volcanic rocks, and a SHRIMP $^{206}Pb/^{238}U$ zircon date for one of several rhyolite dikes present at Alunite Ridge and Deer Trail Mountain, Utah. Both the magmatic-steam alunite and rhyolite dikes are related to concealed intrusions. The rhyolite dike yielded an age of 30.72 ± 0.36 Ma, which is older than a commonly cited 27.1 Ma age estimate for the Three Creeks Tuff Member of the Bullion Canyon Volcanics that is cut by the dike. $^{40}Ar/^{39}Ar$ data for samples of magmatic-steam alunite and sericite from six mines and prospects provide evidence for at least two periods of episodic hydrothermal activity at ca. 15.7–15.1 Ma and ca. 14.7–13.8 Ma, with the older and younger pulses of activity recorded at the more eastern and western sites, respectively. These two periods of hydrothermal activity are consistent with previous interpretations that Alunite Ridge and Deer Trail Mountain are underlain by two concealed porphyry stocks. $^{40}Ar/^{39}Ar$ analyses of individual bands in a sample of massive, centimeter-scale banded vein alunite yield indistinguishable ages with a weighted mean of 13.98 ± 0.12 Ma, consistent with a short-lived ($\lesssim$250 ka) magmatic event with episodic vapor discharge recurring on short timescales ($\lesssim$36 ka). $^{40}Ar/^{39}Ar$ geochronology of magmatic-steam alunite is a valuable tool to constrain the timing and duration of magmatic hydrothermal activity associated with unexposed intrusions and potentially porphyry deposits, and therefore may be useful in exploration.

Keywords: magmatic-steam alunite; $^{40}Ar/^{39}Ar$ geochronology; porphyry deposit; hydrothermal activity; SHRIMP U/Pb geochronology; carbonate replacement deposit

Citation: Mercer, C.M.; Cosca, M.A.; Hofstra, A.H.; Premo, W.R.; Rye, R.O.; Landis, G.P. $^{40}Ar/^{39}Ar$ Geochronology of Magmatic-Steam Alunite from Alunite Ridge and Deer Trail Mountain, Marysvale Volcanic Field, Utah: Timing and Duration of Miocene Hydrothermal Activity Associated with Concealed Intrusions. *Minerals* **2022**, *12*, 1533. https://doi.org/10.3390/min12121533

Academic Editor: Nuo Li

Received: 21 September 2022
Accepted: 25 November 2022
Published: 29 November 2022

1. Introduction

Porphyry and epithermal deposits are the most significant global resources for copper (Cu), molybdenum (Mo), and rhenium (Re), and are major sources of gold (Au), silver (Ag), tellurium (Te), selenium (Se), mercury (Hg), and other metals [1]. Both types of deposits are hydrothermal in origin; high-temperature (700–350 °C) porphyry deposits generally form at depths between 2 and 10 km from predominantly magmatic fluids,

while low-temperature (ca. 300–150 °C) epithermal deposits form at depths <1.5 km from mixtures of magmatic and meteoric fluids [1,2]. Multiple lines of evidence from intermineral intrusions (where preserved; [3]), numerical modeling (e.g., [4,5]), and geochronologic studies (e.g., [6–10]) indicate that the timing and duration of (potentially episodic) magmatic and hydrothermal activity are generally closely linked, though under some conditions (e.g., depending on the permeability of the host rocks and the size of the primary intrusion) hydrothermal systems may persist for nearly 1 Ma after an episode of magmatism. In addition, numerical modeling of porphyry Cu systems indicates that the overall volume and duration of magmatic (and, therefore, hydrothermal) activity is the primary control on the endowment of a deposit [5], with secondary factors such as the efficiency of ore mineral precipitation contributing to the variability of endowment observed in particular types of porphyry deposits (e.g., Au-rich porphyry deposits; [11]). If these controls also apply to other types of porphyry deposits (e.g., Climax-type Mo deposits), then high-precision geochronology (e.g., $^{40}Ar/^{39}Ar$) to establish the timing and duration of magmatic and hydrothermal activity in epithermal deposits is a powerful exploration tool for concealed porphyry deposits.

Most actively mined deposits have been exhumed such that the ore bodies are relatively close to the surface and economically extractable. More deeply buried and undiscovered porphyry systems may have hydrothermal alteration halos that extend to the surface. Alunite, which forms by a variety of processes in supergene and hypogene environments and is indicative of different types of alteration and/or different types of mineralization, has potential for mineral deposit prospecting, e.g., [12]. Magmatic hydrothermal replacement alunite forms as SO_2 laden magmatic vapor cools and contracts at the top of the magmatic vapor plume and equilibrates with wall rock, with alunite replacing aluminosilicates in the host rocks and disseminated pyrite forming as a result of H_2S in the fluids replacing Fe-bearing minerals. In contrast, magmatic-steam vein alunite forms as highly oxidizing magmatic vapor rapidly expands unimpeded along open fractures all the way to the surface without significant interaction with wall rock [12]. Vein alunite generally precipitates as banded sequences of fine-grained to dendritic to terminated crystals growing from the fracture walls towards the center, with trace to locally minor amounts of hematite.

Both types of alunite can constrain the timing and duration of hydrothermal (and, indirectly, magmatic) activity above concealed intrusions. Published geologic, structural, and geochemical data from Alunite Ridge and Deer Trail Mountain indicate a strong likelihood that a concealed porphyry system is present at depth [13,14]. In this investigation, we analyzed samples of nearly pure magmatic-steam vein alunite (most of which are coarsely crystalline; two are fine-grained) using the $^{40}Ar/^{39}Ar$ method as a means of establishing the timing and duration of magmatic degassing at Alunite Ridge and Deer Trail Mountain, Utah. Here, we document $^{40}Ar/^{39}Ar$ data for magmatic-steam alunite that record at least two periods of episodic hydrothermal activity. We show that magmatic-steam alunite—which formed above two concealed intrusions—records numerous volatile exhalations that occurred over short durations ($\lesssim$250 ka), with a recurrence interval $\lesssim$36 ka. We also test whether age variations are recorded between cm-scale bands of alunite, and place the timing of magmatic-steam alunite within a larger tectonic context of migrating Miocene bimodal magmatic activity following rollback of the previously subducted Farallon slab. We also report a zircon $^{206}Pb/^{238}U$ date for one of several felsic dikes that cut the Bullion Canyon Volcanics at Alunite Ridge and Deer Trail Mountain to explore how these intrusions relate temporally to the concealed porphyry system and potentially to mineralization in the area. Our results demonstrate the utility of high-precision $^{40}Ar/^{39}Ar$ geochronology of alunite as an exploration tool, particularly for locating and characterizing deeply concealed porphyry systems.

2. Geologic Setting

2.1. Magmatic-Steam Alunite at Marysvale, Utah

The Marysvale volcanic field is located in the High Plateaus of Utah where the Colorado Plateau transitions to the Basin and Range (Figure 1). It is situated near the northeastern terminus of a broad belt of Paleogene and Neogene igneous rocks and associated mineral deposits that stretch more than 350 km from southeastern Nevada into central Utah [15]. The Marysvale volcanic field is dominated by an upper Eocene–lower Miocene sequence of calc-alkaline intermediate rocks (andesite to low-silica rhyolite lava flows, ash-flow tuffs, volcanic breccias, and debris flows) erupted between about 35 Ma and 22 Ma, and a Miocene bimodal rhyolite and basalt suite erupted between 22 Ma and 14 Ma (e.g., [16]). These upper Eocene, Oligocene, and Miocene volcanic rocks unconformably overlie Paleozoic, Mesozoic, and lower Cenozoic sedimentary rocks [13]. At Alunite Ridge and Deer Trail Mountain, units of the ca. 34–22 Ma Bullion Canyon Volcanics are exposed atop the older sedimentary rocks (e.g., [17]).

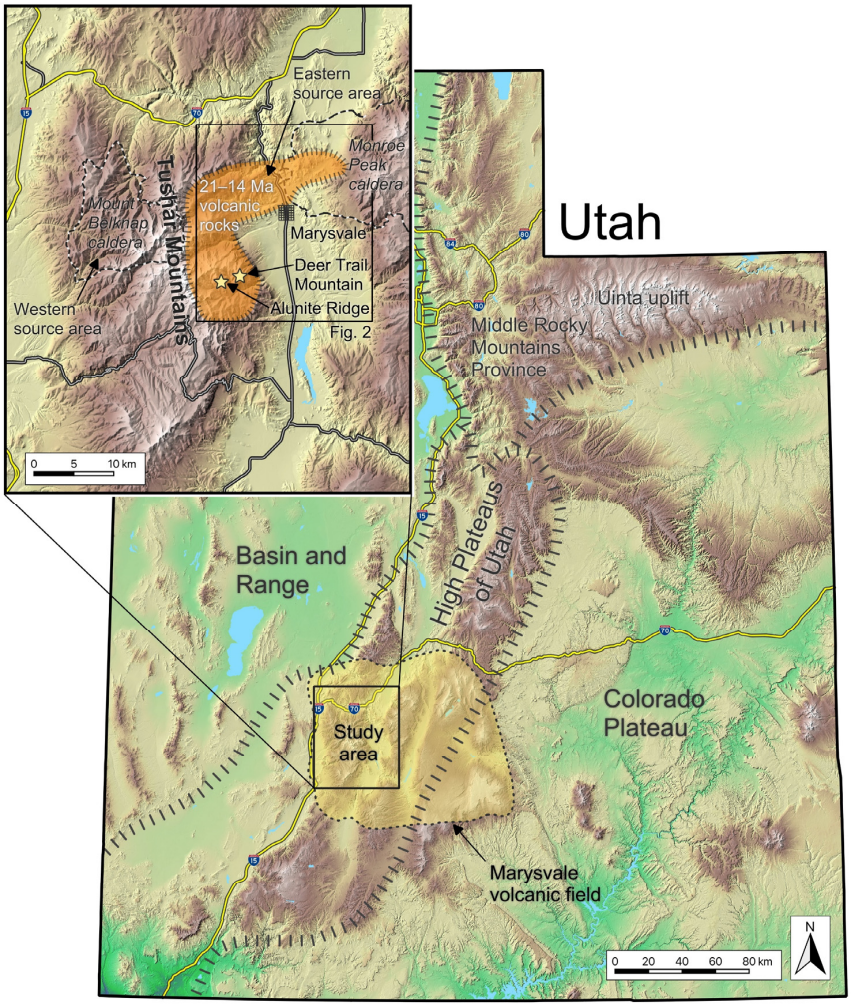

Figure 1. Map of Utah with the location of the Marysvale volcanic field (yellow region with dotted border) highlighted relative to the major physiographic provinces in the region (approximate boundaries shown by hashed lines). The study area is shown in the inset with the boundaries of the Monroe Peak and Mount Belknap calderas indicated by the dashed lines and the approximate region where 21–14 Ma volcanic rocks are exposed indicated by the orange region with the hashed outline. The area of Figure 2 is shown in the inset.

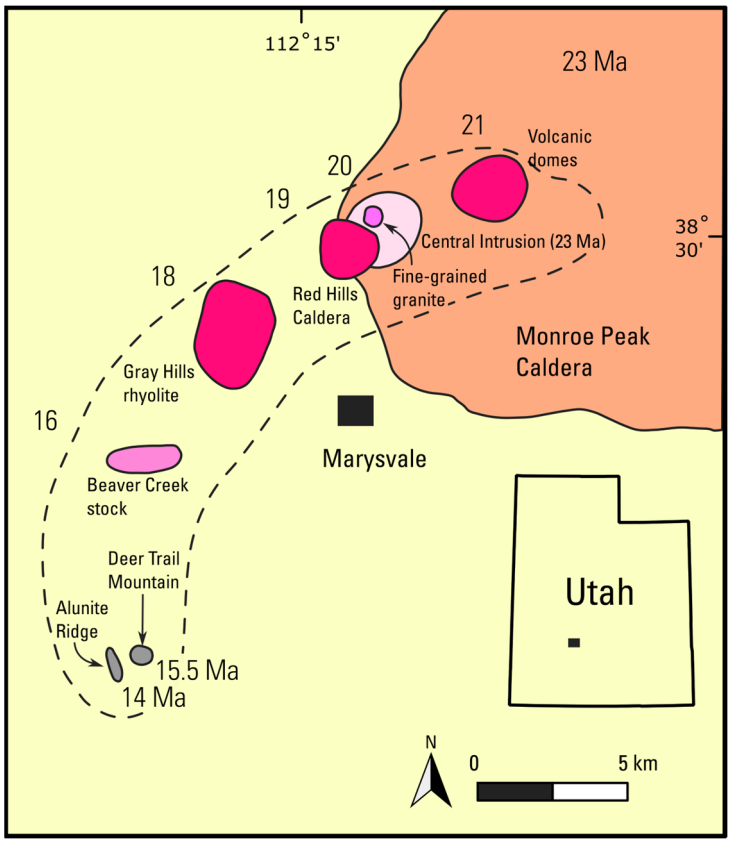

Figure 2. Schematic map showing the spatial and temporal migration of volcanic sources within the eastern source area (indicated by the dashed line) of the Mount Belknap Volcanics in the Marysvale volcanic field. Figure after Cunningham et al. [14] (see also Cunningham et al. [16] for detail of the Central intrusion). See Figure 1 for location.

The rhyolitic rocks of the younger Mount Belknap Volcanics that are exposed in the Marysvale area were erupted from two distinct igneous centers: a western source area dominated by the mostly Oligocene Mt. Belknap caldera located in the central Tushar Mountains, and an elongate (ca. 24 km by 5 km) eastern source area in the Antelope Range that stretches from northeast of Marysvale to Alunite Ridge and Deer Trail Mountain (Figure 1) [13,16]. Igneous activity in the eastern source area began ca. 21–19 Ma northeast of Marysvale with shallow intrusions and the eruption of rhyolite tuffs, then migrated to the southwest over several Ma and culminated in the formation of the Deer Trail Ag–Au–base metal mantos and alunite veins at Alunite Ridge and Deer Trail Mountain, likely associated with the intrusion of two concealed stocks (Figure 2) [13,14,16,18]. However, no bimodal volcanic or intrusive rocks are exposed at Alunite Ridge or Deer Trail Mountain.

Alunite Ridge, located ca. 12 km southwest of Marysvale in the Tushar Mountains (Figures 1 and 2), hosts a series of small mines and excavations including the world's largest known deposits of pure, coarsely crystalline K-alunite in banded veins up to 20 m thick [13]. Mining of K-alunite at Alunite Ridge first began when Germany restricted exports of potash in 1914. Between 1915 and 1920 the principle mine, Mineral Products, produced an estimated 250,000 tons of potash from an estimated 3 million total tons of vein-type alunite. After a hiatus, mining resumed briefly during World War II when an additional 12,000 tons of replacement-type alunite was processed to recover alumina due to a shortage of bauxite for aluminum production [19].

Advanced argillic alteration is common in rocks of the Marysvale area, and replacement- and vein-type alunite formed in distinct epithermal environments and locations [13]. The replacement alunite is fine-grained, and formed in near-surface, highly oxidizing conditions during hydrothermal alteration of volcanic rocks associated with intrusions of

quartz monzonite stocks with published K/Ar and $^{40}Ar/^{39}Ar$ ages of 23–21 Ma [13,15,20]. These replacement deposits are mostly located near the periphery of the Central intrusion (Figure 2) [16], though several smaller deposits are associated with the intrusive core of the Monroe Peak caldera [13].

In contrast to replacement alunite in the Marysvale area, vein-type alunite at Alunite Ridge and Deer Trail Mountain is coarsely crystalline, banded at the centimeter scale, and precipitated from "magmatic steam", which is generally defined as a low-density fluid that ascends rapidly from a degassing magma to shallow levels and that may contain one or two subcritical phases (liquid and vapor; [21]). At Alunite Ridge, magmatic-steam alunite filled extensional fractures to form veins that are steeply dipping and cut through the previously erupted dacitic rocks of the Bullion Canyon Volcanics, and cut or parallel rhyolitic quartz-porphyry dikes of unknown age. Some of the alunite veins are enveloped by magmatic hydrothermal replacement alunite. The vein alunite (and associated enveloping replacement alunite, where present) is likely genetically related to two inferred stocks beneath Alunite Ridge and Deer Trail Mountain. These intrusions produced concentric and radial fractures superposed on regional (generally N–S to NE–SW trending) Basin and Range structures and zoned alteration halos that are most intense at Alunite Ridge and generally grade outward from advanced argillic alteration to propylitic alteration [13,14]. The vein alunite contains gas-rich fluid inclusions, indicating precipitation from a low-density SO_2-rich vapor that had little interaction with the wall rocks, and S, H, and O-isotope data indicate a magmatic origin of the steam with no significant isotopic exchange with the wall rocks (e.g., as evidenced by disequilibrium $d^{34}S$ compositions) or meteoric water [12,13,21,22]. In comparison, typical replacement alunite in Marysvale area (and worldwide) has relatively gas-poor fluid inclusions (with fluids formed from more dense, relatively SO_2-poor and H_2S-rich fluids) and isotopic compositions (e.g., for $d^{34}S$) that more closely approach equilibrium conditions [12,21].

Bassett et al. [23], Caskey and Shuey [24], and Steven et al. [15] reported K/Ar dates for numerous igneous rocks, alunite, and sericite in the Marysvale area, including two dates for vein-type alunite from the Mineral Products mine of 14.3 ± 0.6 (0.7) Ma and 13.8 ± 0.6 (0.7) Ma (2σ, Table S1). (If available, we show external uncertainties, which include decay or decay plus monitor age uncertainties for K/Ar and $^{40}Ar/^{39}Ar$ dates, in parentheses following internal uncertainties for each date in the paper.) The samples of sericite studied by Bassett et al. [23] were collected from the Deer Trail mine workings, and indicate hydrothermal activity altered the Permian country rocks at ca. 14.6–13.2 Ma. The data reported by Caskey and Shuey [24] and Steven et al. [15] include dates for the Three Creeks Tuff Member of the Bullion Canyon Volcanics and the underlying Wah Wah Springs Tuff Member of the Needles Range Group, which have been interpreted (along with zircon fission track dates) as indicating the Three Creeks Tuff Member is ca. 27.1 Ma [15,25]. More recently, Best et al. [26] published a weighted mean of 11 plateau dates of 30.06 ± 0.10 (0.16) Ma (2σ) for plagioclase separates from samples of the Wah Wah Springs Tuff Member (Table S2). Waltenberg [27] and Ren and Vasconcelos [28] analyzed several neutron-irradiated aliquots of one sample of coarsely crystalline pink alunite from Alunite Ridge (Berkeley mineral collection, sample number 5915) to study Ar diffusion and ^{39}Ar recoil effects in alunite. Because the samples had been irradiated, they were also able to compute plateau $^{40}Ar/^{39}Ar$ dates ranging from 15.96 ± 0.11 (0.12) Ma to 15.553 ± 0.072 (0.081) Ma (2σ, Table S2). (The K/Ar and $^{40}Ar/^{39}Ar$ dates cited here have been recalculated using decay, isotopic, and monitor age parameters consistent with those we used to compute our results; see Methods for details.)

2.2. Current Mineral Exploration at Deer Trail

At the time of writing this manuscript, MAG Silver Corp. holds most of the land and claims around Deer Trail Mountain and Alunite Ridge. The company is actively exploring for carbonate replacement deposits (CRD) at the Deer Trail mine. They have completed an initial drilling campaign in which they confirmed the presence of the Redwall Limestone

(a favorable lithology for the formation of CRDs), traced feeder structures to depth, and intercepted high-grade sulfide mineralization within host rocks at greater depths than was previously known [29]. All three of the holes that were drilled as part of this initial campaign bottomed out in "multi-phase porphyritic granitoids" [29], which may be part of one of the hypothesized porphyry stocks. The age of the porphyritic granitoid rocks has not yet been reported. A second phase of drilling is currently underway. We also note that geologists at MAG Silver Corp. have sampled "felsite" dikes from their property around Alunite Ridge and Deer Trail Mountain, and reported U/Pb and $^{40}Ar/^{39}Ar$ dates ranging from 31–28 Ma, though detailed analytical data are not yet available [30]. From publicly available images and limited access by the authors to hand specimens, these "felsite" dikes appear to have similar coloration, mineralogy, and textures to the quartz-porphyry dikes we have observed in the field at the Mineral Products, Christmas, and Bradburn mines.

3. Materials and Methods

3.1. Samples

Samples of vein-type magmatic-steam alunite were collected over multiple field seasons from veins exposed at four alunite mines and workings, and at a mine dump at the Close In landslide deposit, which slid from the top of Deer Trail Mountain and is currently located at the edge of the Sevier Valley to the northwest of the Deer Trail mine and on the eastern side of the Tushar fault [19]. These include: three samples (M939-1, M939A, M945) of magmatic-steam alunite from the upper Mineral Products mine taken from a ca. 20 m-wide vein crosscutting altered rhyolite at a high angle; four samples (002-05, 003-05, Edna 2a Fine, and Edna 3a Coarse) from the Mt. Edna prospect; two samples (005-08 and 21AR01) from the L&N locality; two samples (Close In and ROR MV-1-06) from the Close In mine dump at the edge of the Sevier Valley; and three samples (21AR03 Coarse, 21AR03 Fine, and a banded slab of alunite M341 from a 0.5 m-wide vein) from the Christmas mine (Figure 3, Table S3).

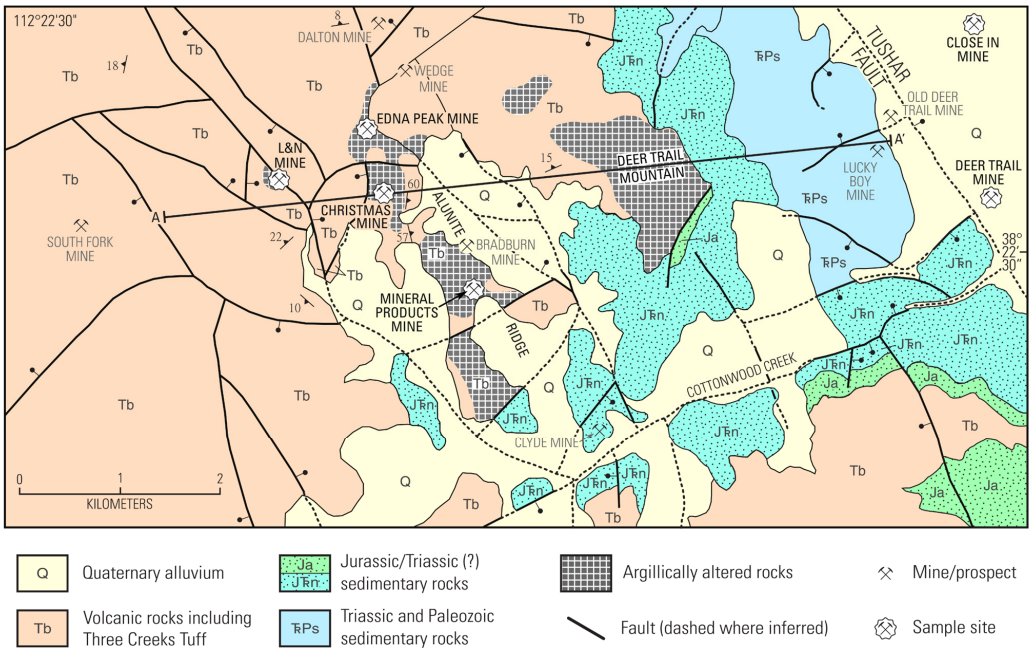

Figure 3. Simplified geologic map with mine locations of Alunite Ridge and Deer Trail Mountain, Marysvale, Utah (modified after Beaty et al. [14]). A felsic dike was collected from the upper Mineral Products mine for zircon U/Pb analyses. Samples of magmatic-steam alunite were collected from the L&N, Christmas, Edna, Mineral Products, and Close In mines/prospects, and sericite was separated from a sample collected from the Deer Trail mine workings for $^{40}Ar/^{39}Ar$ dating. Note, the location shown for the Deer Trail mine marks the portal to the workings, which extend ca. 3200 m to the west beneath Deer Trail Mountain [14]. The cross section from A to A′ is shown in Figure 9.

Aliquots of all samples except ROR MV-1-06 and 002-05, including twelve individual aliquots extracted from seven of the bands in the alunite slab (M341), were analyzed using the incremental heating $^{40}Ar/^{39}Ar$ method at the U.S. Geological Survey (USGS) in Denver, CO. Aliquots of M939A, ROR MV-1-06, and 002-05 were analyzed using the single-grain total fusion (SGTF) $^{40}Ar/^{39}Ar$ method, also at the USGS in Denver. All aliquots of alunite were prepared for $^{40}Ar/^{39}Ar$ analysis by gently crushing the coarse- and fine-grained alunite specimens, washing in deionized water, and hand-picking fresh mm- and sub-mm-sized fragments under a binocular microscope. A sample (M992) was also collected from the workings of the Deer Trail mine (Figure 3, Table S3) from which sericite was separated by physically scraping mineral surfaces and interiors of vugs. Three separates of sericite were analyzed by the incremental heating $^{40}Ar/^{39}Ar$ method at the USGS in Denver.

A sample of a highly altered N30°W-trending rhyolitic quartz-porphyry dike (M945-R) was also taken from the upper Mineral Products mine at the same location as the alunite sample M945 (Figure 3, Table S3) to determine the timing of this generation of intrusive activity relative to the hydrothermal system that produced the magmatic-steam alunite (and potentially produced the CRD at the Deer Trail mine [13,14]). This felsic dike shares one contact with the host rocks of the Three Creeks Tuff Member of the Bullion Canyon Volcanics [31], and one contact with the vein alunite that formed parallel to the rhyolitic dike. Sample M945-R was, crushed, pulverized, and sieved to obtain the 32–200 mesh fraction, which was then processed to concentrate zircon by density separation with methylene iodide (ρ = 3.32 g/cm^3). The "heavies" were briefly washed in acetone, followed by a final Frantz magnetic separation. The zircons were not air-abraded or acid-washed during preparation for U-Pb analyses. Approximately 60 grains were handpicked under a binocular microscope for inclusion onto an epoxy mount. The mount was ground to expose the approximate center of the grains, polished, and then imaged with transmitted light, reflected light, and cathodoluminesence (CL) to identify internal structures, zoning related to chemical composition, and defects. CL imaging (Figure S65) was performed on the JEOL 5800 scanning electron microscope at the USGS Microbeam Laboratory, Denver. Nine zircon grains from M945-R were analyzed for U-Th-Pb isotopic values, and U-Th-Pb, REE, and Hf concentrations on the SHRIMP-RG at the Stanford-USGS Micro Analysis Center (SUMAC) at Stanford University.

3.2. $^{40}Ar/^{39}Ar$ Geochronology Methods

Selected alunite fragments and sericite separates were loaded along with the neutron fluence monitor Fish Canyon sanidine (FCs) into precise positions within 18 mm-diameter Al disks, stacked, wrapped in high-purity Al foil and encapsulated under vacuum in quartz tubes. The quartz tubes were sealed into Al canisters with Cd shielding to reduce thermal neutron interactions and rotated at 1 rpm during six separate neutron irradiations (DT-2 and DT-4 each totaled 20 MWh; DT-6 totaled 10 MWh; DT-7 totaled 1 MWh; DT-11 totaled 2 MWh; DT-47 totaled 6 MWh; Table S4) in the central thimble position of the USGS TRIGA reactor [32]. Following irradiation, the alunite and sericite samples and grains of the FCs neutron fluence monitor were loaded with stainless-steel tweezers into a stainless-steel or copper sample holder and placed into a laser chamber with an externally pumped ZnSe window, which is attached to a custom-built ultra-high vacuum extraction line. For alunite analyses, pure silver wool was inserted into the exit tube of the sample chamber to react with any free sulfur gas liberated during sample heating. The volume of the mostly stainless-steel extraction line, including a cryogenic trap operated at −130 °C and two SAES GP50 getters (one operated at room temperature, one operated at 2.2A), is estimated at ~450 cc. A combination of turbo molecular pumps and ion pumps maintain steady pressures within the extraction line of $<1.33 \times 10^{-7}$ Pa.

Individual alunite fragments were either incrementally heated or fused in a single extraction by controlling the power output of a 50 W CO_2 laser equipped with a beam homogenizing lens, which results in uniform energy deposition over the entire sample surface. Aliquots of sericite were incrementally heated. During laser heating (for durations

between 20 and 90 s), the gas evolved from the sample was exposed simultaneously to the silver wool (alunites only) and the cryogenic trap, and the gas was further purified in a second stage by additional exposure to the SAES getters for 120 s. For samples analyzed in 2009–2011, the sample gas was then expanded into a Mass Analyzer Products (MAP) 215-50 noble gas mass spectrometer in static vacuum mode. Isotopes were measured using an electron multiplier detector operating in analog mode by sequentially peak hopping over the mass range 36 to 40 for 10 cycles of data collection on each isotope. The MassSpec computer program written by A. Deino of the Berkeley Geochronology Center was used for data acquisition (v. 7.76). For samples analyzed in 2022, purified sample gases were expanded into a Thermo Scientific Argus VI noble gas mass spectrometer in static vacuum mode. Isotopes were simultaneously collected using four Faraday cups (for masses 40, 39, 38, and 37 on H1, AX, L1, and L2, respectively) and one compact discrete dynode (CDD) secondary electron multiplier detector (for mass 36). The Faraday detectors were intercalibrated by peak hopping a beam of ^{40}Ar over each detector using an automated routine in MassSpec (v. 7.91); the CDD was intercalibrated relative to the H1 Faraday cup using the Isotopic Reference Ratio Intercalibration (IR-IC) method [33] where the measured $^{40}Ar_{H1}/^{36}Ar_{CDD}$ ratio is calibrated to the atmospheric value of 298.56 ± 0.31 (1σ) [34].

All data reduction was performed with MassSpec (v. 8.159). Time zero intercepts were fit to the data (using parabolic, linear, and/or average best fits) and corrected for detector baselines, operational blanks (where the instrument was run as if to analyze a sample, but without firing the laser), mass discrimination (for peak hopping data collected on the MAP 215-50, monitored by analyzing air pipettes) or combined detector intercalibration/mass bias (for data multicollected on the Argus VI, using air pipette analyses and the IR-IC method of Turrin et al. [33]), radioactive decay of ^{37}Ar and ^{39}Ar, and nucleogenic interferences. Apparent ages for SGTF grains and steps in incremental heating experiments were also corrected for trapped atmosphere (see additional details below).

Laser fusion of individual FCs crystals at each position within the irradiation packages resulted in neutron flux ratios reproducible to ≤1.1%, with most ≤0.5% (2σ). Isotopic production ratios were determined from irradiated CaF_2 and KCl salts; $(^{36}Ar/^{37}Ar)_{Ca}$, $(^{38}Ar/^{37}Ar)_{Ca}$, $(^{39}Ar/^{37}Ar)_{Ca}$, $(^{40}Ar/^{39}Ar)_{K}$, and $(^{38}Ar/^{39}Ar)_{K}$ values are given in Table S5. Cadmium shielding during irradiation prevented any measurable $(^{40}Ar/^{39}Ar)_{K}$. $^{40}Ar/^{39}Ar$ plateau dates (and uncertainties) are considered the best estimate of the cooling age of the minerals and were calculated from samples if three or more consecutive heating steps released ≥50% of the total $^{39}Ar_{K}$ and that had indistinguishable apparent $^{40}Ar/^{39}Ar$ ages at 2σ [35]. In a few instances where the Fleck et al. [35] algorithm did not identify a plateau, we forced a plateau for exploratory purposes but prefer the integrated (total gas) dates in these cases. $^{40}Ar/^{39}Ar$ plateau and total gas (integrated) dates are reported in Table 1 (see Figures S1–S29), which were computed using an age of 28.201 ± 0.012 (0.046) Ma for FCs (2σ; [36]), the ^{40}K decay constants of Min et al. [37], and an atmospheric $^{40}Ar/^{36}Ar$ ratio of 298.56 ± 0.31 (1σ) [34]. Note, all K/Ar and $^{40}Ar/^{39}Ar$ dates quoted from the literature have been recalculated to use decay, isotopic, and monitor age parameters that are consistent with the Min et al. [37] decay constants and the age for FCs of Kuiper et al. [36] using the *ArAR* tool of Mercer and Hodges [38]. For the parameters used here, the effects of recalculating most published K/Ar and $^{40}Ar/^{39}Ar$ dates are well below the reported uncertainties, with age shifts of ≤0.2% and <0.005%, respectively (Tables S1 and S2). The only exceptions are for two K/Ar dates of sericite reported by Bassett et al. [23] and two K/Ar dates of biotite reported by Caskey and Shuey [24], which were shifted by ca. 2.80%–2.84% when recomputed with our preferred decay and isotopic parameters (Table S1).

Dates for SGTF analyses were pooled for each sample to compute an inverse variance-weighted mean (hereafter simply a "weighted mean"; Table 2, Figures S30–S32). Where the *MSWD* fell outside of the 95% CI of the *MSWD* distribution, we performed outlier detection using an algorithm based on the Hampel identifier, which is based on deviations from the median rather than the mean (e.g., for more commonly applied Extreme Studen-

tized Deviation or "2-sigma exclusion" identifiers) [39] (pp. 280–311). Here, we applied the Hampel identifier to the

$$\chi_i^2 = \frac{\left(x_i - \bar{x}\right)^2}{\sigma_i^2} \quad (1)$$

values (where x_i and σ_i are the value and uncertainty of each date, respectively, and $\bar{x}$ is the weighted mean), which are effectively the weighted residuals of the individual dates from the weighted mean. Thus, the analytical uncertainties of each date influence the identification of outliers, since relatively precise dates have a stronger effect on the value of the weighted mean than more imprecise dates. For each sample, we started with a permissive cutoff value of 6 (beyond which the OLi values computed using the Hampel identifier are considered potential outliers) and then moved in integer steps to lower, more aggressive cutoff values to identify the fewest number of outliers necessary to achieve an acceptable $MSWD$ or until we reached a cutoff value of 2. (Note, in some cases relatively imprecise dates on the margins of a population can be retained by this process while more precise dates closer to the center of the distribution can be identified as potential outliers).

Table 1. Summary of plateau and total gas $^{40}Ar/^{39}Ar$ dates for samples of magmatic-steam alunite from Alunite Ridge, and sericite from the Deer Trail mine workings, Marysvale, Utah. Preferred ages are in bold. Age uncertainties are provided at both the 1σ and 95% confidence (95% CI) levels, and include the error in J; external uncertainties (denoted by a subscript x) also include decay constant uncertainties. Dates have been rounded to the same decimal place as the 95% CI (internal) uncertainties, which are rounded to 2 significant figures. Acceptable *MSWD* values fall within the 95% confidence intervals computed following the methods of Mahon, 1996 [40]. Where the *MSWD* values are unacceptable, the 95% CIs (internal and external) of the ages have been expanded by $\sqrt{MSWD}$ and are denoted with an X in the Xpnd column; the 1σ uncertainties are provided without expansion.

Sample	Mine/Prospect	Lab Run ID	Plateau											Total Gas								
			Age (Ma)											Age (Ma)								
			t	1σ	$1\sigma_x$	95% CI	95% CI_x	Xpnd	$\%^{39}Ar_K$	N	*MSWD*	95% CI (*MSWD*)	Algorithm	t	1σ	$1\sigma_x$	95% CI	95% CI_x	Xpnd	N	*MSWD*	95% CI (*MSWD*)
Magmatic-steam alunite data collected on MAP 215-50																						
003-05	Mt. Edna prospect	112-01	**13.1**	0.38	0.45	**1.0**	1.2		100.0	5	0.997	[0.121, 2.79]	Fleck, 1977	13.1	0.38	0.45	1.0	1.2		5	0.997	[0.121, 2.79]
005-08	L&N mine	108-01	**14.02**	0.39	0.47	**0.93**	1.1		100.0	8	0.289	[0.241, 2.29]	Fleck, 1977	14.02	0.39	0.47	0.93	1.1		8	0.289	[0.241, 2.29]
M341 A′	Christmas mine	307-01	**14.20**	0.080	0.27	**0.21**	0.70		71.7	6	1.52	[0.166, 2.57]	Fleck, 1977	14.21	0.079	0.27	0.31	1.1	X	13	3.32	[0.367, 1.94]
M341 A2	Christmas mine	109-01	**13.3**	0.37	0.44	**1.0**	1.2		100.0	5	1.28	[0.121, 2.79]	Fleck, 1977	13.3	0.37	0.44	1.0	1.2		5	1.28	[0.121, 2.79]
M341 B1	Christmas mine	308-02	**14.11**	0.085	0.27	**0.20**	0.63		100.0	9	1.17	[0.272, 2.19]	Fleck, 1977	14.11	0.085	0.27	0.20	0.63		9	1.17	[0.272, 2.19]
M341 B2	Christmas mine	309-01	**13.97**	0.079	0.27	**0.19**	0.65		98.8	7	1.22	[0.206, 2.41]	Fleck, 1977	13.97	0.079	0.27	0.32	1.1	X	8	2.95	[0.241, 2.29]
M341 B3	Christmas mine	310-01	**14.28**	0.13	0.29	**0.30**	0.65		98.9	11	1.23	[0.325, 2.05]	Fleck, 1977	14.28	0.13	0.29	0.29	0.64		13	1.84	[0.367, 1.94]
M341 C2	Christmas mine	311-01	**13.85**	0.14	0.29	**0.35**	0.71		92.6	7	0.676	[0.206, 2.41]	Fleck, 1977	13.85	0.14	0.29	0.31	0.63		13	1.62	[0.367, 1.94]
M341 D1	Christmas mine	302-01	**13.95**	0.079	0.27	**0.17**	0.59		100.0	12	0.682	[0.347, 1.99]	Fleck, 1977	13.95	0.079	0.27	0.17	0.59		12	0.682	[0.347, 1.99]
M341 D2	Christmas mine	110-01	**16.1**	2.1	2.1	**5.5**	5.5		100.0	6	0.706	[0.166, 2.57]	Fleck, 1977	16.1	2.1	2.1	5.5	5.5		6	0.706	[0.166, 2.57]
M341 D3	Christmas mine	304-01	**13.78**	0.080	0.26	**0.26**	0.84		73.1	4	1.33	[0.0719, 3.12]	Fleck, 1977	13.78	0.079	0.26	0.18	0.59		11	1.67	[0.325, 2.05]
M341 E2	Christmas mine	306-01	**13.94**	0.072	0.26	**0.18**	0.68		95.8	6	0.674	[0.166, 2.57]	Fleck, 1977	13.94	0.071	0.26	0.25	0.91	X	9	2.23	[0.272, 2.19]
M341 F2	Christmas mine	111-01	**13.89**	0.19	0.32	**0.48**	0.81		100.0	6	0.930	[0.166, 2.57]	Fleck, 1977	13.89	0.19	0.32	0.48	0.81		6	0.930	[0.166, 2.57]
M341 G2	Christmas mine	312-01	**13.62**	0.16	0.29	**0.35**	0.66		100.0	11	0.852	[0.325, 2.05]	Fleck, 1977	13.62	0.16	0.29	0.35	0.66		11	0.852	[0.325, 2.05]
M939-1	Upper Mineral Products mine	429-01	**15.67**	0.10	0.30	**0.29**	0.85		53.0	5	1.73	[0.121, 2.79]	Fleck, 1977	15.81	0.10	0.30	0.55	1.7	X	14	6.90	[0.385, 1.90]
M945	Upper Mineral Products mine	495-01	**15.83**	0.12	0.31	**0.26**	0.69		100.0	12	0.294	[0.347, 1.99]	Fleck, 1977	15.83	0.12	0.31	0.26	0.69		12	0.294	[0.347, 1.99]

Table 1. *Cont.*

Sample	Mine/Prospect	Lab Run ID	Plateau										Total Gas								
			Age (Ma)										Age (Ma)								
			t	1σ	1σ$_x$	95% CI	95% CI$_x$	Xpnd	%^{39}Ar$_K$	N	*MSWD*	95% CI (*MSWD*)	Algorithm	t	1σ	1σ$_x$	95% CI	95% CI$_x$	Xpnd	N	*MSWD*	95% CI (*MSWD*)
Close In	Close In mine dump	431-01	**15.60**	0.11	0.31	**0.24**	0.66		100.0	14	1.77	[0.385, 1.90]	Fleck, 1977	15.60	0.11	0.31	0.24	0.66		14	1.77	[0.385, 1.90]
Magmatic-steam alunite data collected on Argus VI																					
21AR01	L&N mine	2886-01	**14.701**	0.015	0.27	**0.036**	0.64		75.4	8	0.897	[0.241, 2.29]	Fleck, 1977	14.668	0.015	0.27	0.077	1.4	X	15	6.11	[0.402, 1.87]
21AR01	L&N mine	2886-02	14.65	0.015	0.27	0.12	2.2	X	83.2	6	10.2	[0.166, 2.57]	Forced	**14.62**	0.014	0.27	**0.24**	4.5	**X**	13	60.4	[0.367, 1.94]
21AR03 Coarse	Christmas Mine	2888-01	**14.471**	0.015	0.27	**0.035**	0.61		77.4	9	2.08	[0.272, 2.19]	Fleck, 1977	14.44	0.015	0.27	0.11	1.9	X	13	10.9	[0.367, 1.94]
21AR03 Coarse	Christmas Mine	2888-02	**14.462**	0.014	0.27	**0.032**	0.60		92.8	10	1.70	[0.300, 2.11]	Fleck, 1977	14.458	0.014	0.27	0.069	1.3	X	12	4.86	[0.347, 1.99]
21AR03 Fine	Christmas Mine	2887-01	14.29	0.015	0.26	0.21	3.6	X	73.7	4	18.9	[0.0719, 3.12]	Forced	**14.31**	0.015	0.26	**0.19**	3.3	**X**	15	35.2	[0.402, 1.87]
21AR03 Fine	Christmas Mine	2887-02	14.30	0.015	0.26	0.17	2.8	X	82.9	4	11.4	[0.0719, 3.12]	Forced	**14.31**	0.015	0.26	**0.20**	3.4	**X**	10	33.5	[0.300, 2.11]
Edna 2a Fine	Mt. Edna prospect	2891-01	**14.502**	0.016	0.27	**0.069**	1.1		60.2	3	0.669	[0.0253, 3.69]	Fleck, 1977	14.47	0.015	0.27	0.14	2.6	X	11	18.6	[0.325, 2.05]
Edna 2a Fine	Mt. Edna prospect	2891-02	**14.658**	0.019	0.27	**0.043**	0.62		98.1	9	0.966	[0.272, 2.19]	Fleck, 1977	14.658	0.019	0.27	0.066	0.95	X	10	2.45	[0.300, 2.11]
Edna 3a Coarse	Mt. Edna prospect	2889-01	**14.470**	0.028	0.27	**0.065**	0.61		78.4	9	1.74	[0.272, 2.19]	Fleck, 1977	14.50	0.026	0.27	0.10	1.1	X	13	3.34	[0.367, 1.94]
Edna 3a Coarse	Mt. Edna prospect	2889-02	**14.47**	0.053	0.27	**0.13**	0.64		84.7	8	0.697	[0.241, 2.29]	Fleck, 1977	14.46	0.053	0.27	0.12	0.62		9	1.99	[0.272, 2.19]
Close In	Close In mine dump	2892-01	**15.153**	0.025	0.28	**0.058**	0.64		54.1	9	0.461	[0.272, 2.19]	Fleck, 1977	15.117	0.022	0.28	0.075	1.0	X	13	2.56	[0.367, 1.94]
Close In	Close In mine dump	2892-02	**15.288**	0.021	0.28	**0.068**	0.89		60.0	4	1.78	[0.0719, 3.12]	Fleck, 1977	15.287	0.019	0.28	0.044	0.65		9	2.16	[0.272, 2.19]
Deer Trail sericite data collected on Argus VI																					
M992 B1	Deer Trail mine workings	665-01	**15.43**	0.093	0.30	**0.21**	0.67		100.0	10	1.47	[0.300, 2.11]	Fleck, 1977	15.43	0.093	0.30	0.21	0.67		10	1.47	[0.300, 2.11]
M992 B3	Deer Trail mine workings	666-01	**15.400**	0.042	0.28	**0.090**	0.61		82.6	16	1.27	[0.417, 1.83]	Fleck, 1977	15.47	0.039	0.28	0.14	1.0	X	19	2.79	[0.457, 1.75]
M993 D1	Deer Trail mine workings	667-01	**15.643**	0.040	0.29	**0.087**	0.64		73.3	12	1.38	[0.347, 1.99]	Fleck, 1977	15.57	0.037	0.29	0.19	1.5	X	18	6.11	[0.445, 1.78]

Table 2. Summary of inverse variance-weighted mean $^{40}Ar/^{39}Ar$ dates for samples of magmatic-steam alunite from Alunite Ridge, Marysvale, Utah. Preferred ages are in bold. Age uncertainties are provided at both the 1σ and 95% confidence (95% CI) levels, and include the error in J; external uncertainties (denoted by a subscript x) also include decay constant uncertainties. Dates have been rounded to the same decimal place as the 95% CI (internal) uncertainties, which are rounded to 2 significant figures. Acceptable *MSWD* values fall within the 95% confidence intervals computed following the methods of Mahon, 1996 [40]. Where the *MSWD* values are unacceptable, the 95% CIs (internal and external) of the ages have been expanded by $\sqrt{MSWD}$ and are denoted with an X in the Xpnd column; the 1σ uncertainties are provided without expansion.

Sample	Mine/Prospect	Lab Run ID	Inverse Variance-Weighted Mean								
			Age (Ma)								
			t	1σ	$1\sigma_x$	95% CI	95% CI_x	Xpnd	N	*MSWD*	95% CI (*MSWD*)
	Data collected on Argus VI										
002-05	Mt. Edna prospect	2894	**14.349**	0.0163	0.26	**0.033**	0.54		27	1.35	[0.532, 1.61]
M939A	Upper Mineral Products mine	2893	**15.445**	0.0089	0.28	**0.018**	0.59		23	1.25	[0.499, 1.67]
ROR MV-1-06	Close-In mine dump	2921	**15.262**	0.0073	0.28	**0.020**	0.75	**X**	24	1.68	[0.508, 1.66]

We also computed inverse isochrons for each sample of alunite (Table S6, Figures S33–S61). (We did not compute inverse isochrons for aliquots of Deer Trail sericite since all the evolved gasses were dominated by radiogenic ^{40}Ar.) Alunite data were excluded from York regressions (implemented following York et al. [41]) if they represented <2% of the total $^{39}Ar_K$ released or had ^{36}Ar signals that were indistinguishable from the background (one step from M341 G2). We consider SGTF weighted mean, plateau, and isochron dates to be acceptable if the value of the mean squared weighted deviation (*MSWD*; [42]) falls within the 95% CI of the *MSWD*, which is sensitive to the degrees of freedom (DOF) in the calculation [40]. In instances where the value of the *MSWD* falls outside the 95% CI of the *MSWD*, we have expanded the uncertainties by $\sqrt{MSWD}$ under the assumption that the uncertainties of individual steps should explain the scatter of data about the SGTF weighted means and plateaus (DOF = N − 1) or York regressions for inverse isochrons (DOF = N − 2).

3.3. SHRIMP U/Pb Geochronology Methods

Prior to SHRIMP-RG analysis, the epoxy mount with zircon grains from M945-R was acid-washed (1N HCl), rinsed (distilled water), dried, and coated with 10 nm of Au for maximum surface conductivity. Using a ~4–6 nA primary O_2 ion beam, a 50 × 70 μm region was rastered for 120 s prior to each analysis. Sensitivity ranged from 5 to 30 cps per ppm Pb. Analysis time ranged from 14 to 16 min with the primary beam producing clean, sharp, 20 to 30 μm elliptical, 1 to 2 μm deep, flat-bottomed, analytical pits. Element concentration data were standardized against zircon standard MAD 4.6 (4200 ppm U; Madagascar green zircon) and are accurate to better than 10 percent, and age-data were standardized against zircon standard R33 (419.26 ± 0.39 Ma, 95% confidence level; from the Braintree Complex monzodiorite, Vermont; [43]), analyzed approximately every fifth analysis. Our foremost objective during the SHRIMP analyses was to measure zones of primary magmatic growth (i.e., to determine the crystallization age). However, we also measured zircon cores and rims (where identified with CL) to define possible ages of inheritance and metamorphic growth. The choice of location of an individual SHRIMP analysis was determined by factors including CL zoning pattern, absence of imperfections such as cracks or inclusions (liquid or solid), and purpose of the analysis (i.e., age of inheritance [source], igneous protolith, and/or metamorphic overgrowth). All analyses were conducted on a single epoxy mount during one analytical session, and no age inconsistencies were observed that could be related to instrument condition nor calibration.

Data reduction followed the methods of Williams [44] and Ireland and Williams [45], using SQUID 1 [46]. We computed a conventional inverse variance-weighted mean using the individual $^{206}Pb/^{238}U$ dates for individual spot analyses (using the methods applied to SGTF $^{40}Ar/^{39}Ar$ data). Both internal (analytical + ^{238}U decay constant) and external uncertainties (also including the age uncertainty of the standard R33) are provided for the weighted mean $^{206}Pb/^{238}U$ date. Rare-earth elements La through Yb and Hf were measured concurrently with the U-Th-Pb analyses as additional masses on each pass through the mass range. The concentration of U, Th, Hf and REE were calibrated using an in-house zircon standard MAD 4.6 and are reproducible at 2%–4% (1σ), except for La (15%) because of its typically very low concentration (30 ppb). Pr was calculated from its neighbor elements because CeH (cerium hydrides) cannot be resolved from the Pr peak and contributes significantly to the counts at ^{141}Pr, given the low abundance of Pr and the relatively higher Ce concentration. Trace element concentrations were normalized to chondrite values of McDonough and Sun [47].

4. Results

$^{40}Ar/^{39}Ar$ results for magmatic-steam alunite and sericite are shown as release spectra (Figure 4, Figures S1–S32) and probability density plots (PDPs, Figures S33–S35); three-isotope correlation (inverse isochron) plots of alunite are provided in the Supplementary Materials (Figures S36–S64); inverse isochrons were not computed for M992 sericite aliquots (released gasses were dominated by radiogenic ^{40}Ar, denoted $^{40}Ar^*$). We report the 95% confidence interval (95% CI) for all ages and discussions below unless otherwise noted. External uncertainties, which include decay and monitor age uncertainties, are shown in parentheses immediately following the internal uncertainties. With few exceptions, the inverse isochron regressions yielded $^{40}Ar/^{36}Ar$ intercepts that are indistinguishable from modern atmosphere. Consequently, isochron dates (Table S6) overlap with the $^{40}Ar/^{39}Ar$ plateau dates summarized in Table 1. Detailed $^{40}Ar/^{39}Ar$ data are tabulated in Table S7.

Samples of magmatic-steam alunite from the upper Mineral Products mine yielded plateau, total gas, and weighted mean dates ranging from 15.83 ± 0.26 (0.69) Ma to 15.445 ± 0.018 (0.59) Ma, and alunite from the Close In locality yielded $^{40}Ar/^{39}Ar$ plateau and weighted mean dates ranging from 15.60 ± 0.24 (0.66) Ma to 15.153 ± 0.058 (0.64) Ma. Our dates for the Mineral Products samples are statistically older than previously determined, but less precise, K/Ar ages (recalculated with decay constants of Min et al. [37]) of 14.3 ± 0.6 (0.7) Ma and 13.8 ± 0.6 (0.7) Ma (2σ) reported by Steven et al. [15] for different samples of vein alunite from the same locality. However, our Close In upper Mineral Products dates are comparable to the ca. 16–15.5 Ma range of dates reported by Waltenberg [27] and Ren and Vasconcelos [28] for multiple aliquots of a sample of vein-type alunite from Alunite Ridge. In addition, sericite from the Deer Trail mine yielded plateaus ranging from 15.643 ± 0.087 (0.64) Ma to 15.400 ± 0.090 (0.61) Ma.

Samples from the L&N locality yielded plateaus and total gas dates ranging from 14.701 ± 0.036 (0.64) Ma to 14.02 ± 0.93 (1.1) Ma. Most samples from the Mt. Edna prospect yielded plateaus and weighted mean dates ranging from 14.658 ± 0.043 (0.62) Ma to 14.349 ± 0.033 (0.54) Ma, while sample 003-05 yielded a comparatively less precise plateau of 13.1 ± 1.0 (1.2) Ma. Samples of coarse-grained and fine-grained vein-type alunite from the Christmas mine yielded dates ranging from 14.471 ± 0.035 (0.61) Ma to 14.31 ± 0.19 (3.3) Ma. In addition, twelve individual aliquots of alunite were analyzed from seven distinct bands of sample M341 from the Christmas mine locality to test for apparent age variations (Figure 5). Two aliquots, A2 and D2, yielded dates that are younger (13.3 ± 1.0 (1.2) Ma) and older (16.1 ± 5.5 (5.5) Ma), respectively, and relatively imprecise compared to dates from the remaining ten aliquots. Note that gas released from aliquot D2 was dominated by atmospheric argon (the median and mean of the $^{40}Ar^*$ yields are 2.5% and 4.7%, respectively; Figure S10), which contributed significantly to the imprecision of the plateau date for D2. The ten aliquots of M341 excluding A2 and D2 yielded overlapping plateau (and isochron) dates ranging from 14.28 ± 0.30 (0.65) Ma to 13.62 ± 0.35 (0.66) Ma (isochrons:

14.19 ± 0.26 (0.72) Ma to 13.54 ± 0.57 (0.82) Ma; Table 1 and Table S6) with a weighted mean of 13.98 ± 0.12 (1.4) Ma (computed from plateau dates; *MSWD* = 3.04, 95% CI expanded by a factor of ca. 1.74; Figure 5). All alunite and sericite dates are shown in Figure 6.

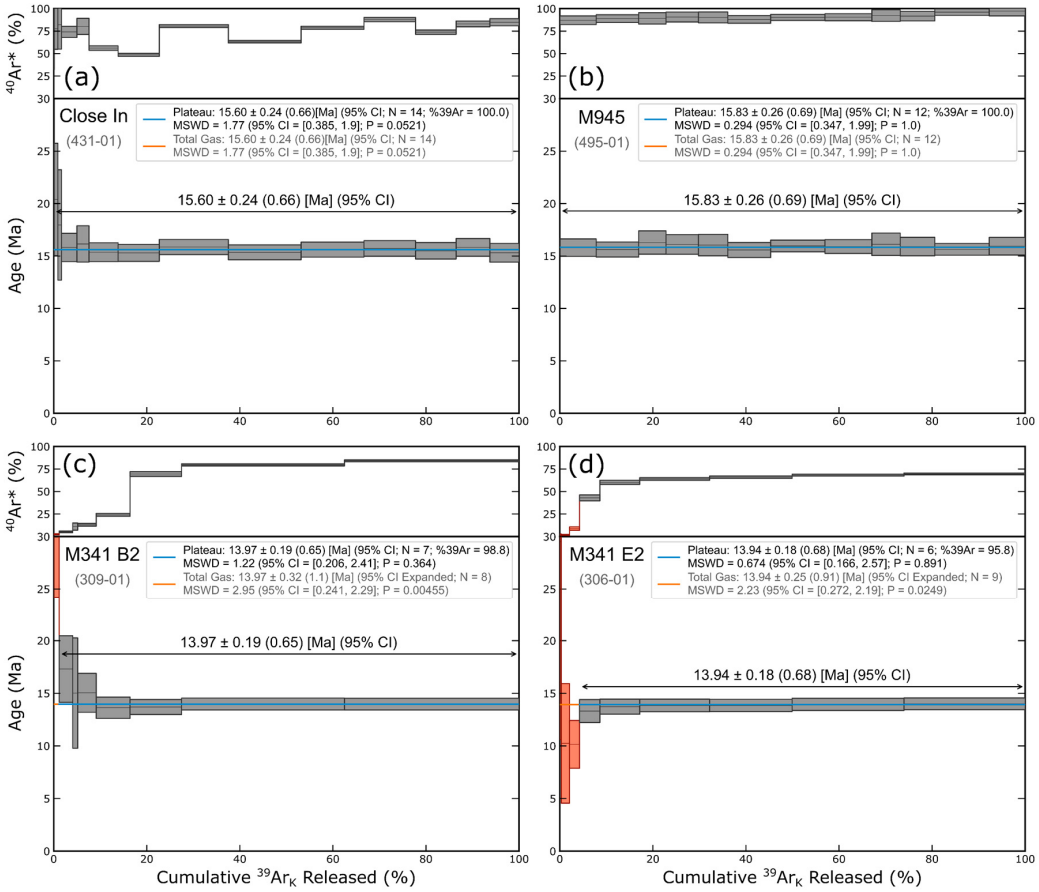

Figure 4. Selected $^{40}Ar/^{39}Ar$ release spectra for samples of magmatic-steam alunite. (**a**,**b**) Results for Close In and M945 representing an older pulse of hydrothermal activity ca. 15.7 Ma. (**c**,**d**) Results for M341 bands B2 and E2 representing a younger pulse of hydrothermal activity ca. 14 Ma. Red steps were excluded from plateau calculations, while both gray and red steps were included when computing total gas dates. External age uncertainties are shown in parentheses after internal uncertainties. The 95% CI of the asymmetric *MSWD* are shown in square brackets in the inset legends; where the value of the *MSWD* falls outside of these bounds, the resulting uncertainties were expanded by $\sqrt{MSWD}$ (this only affected the total gas dates for M341 B2 and E2).

U-Th-Pb isotope data are summarized in Table 3 and illustrated in Figure 7 (see Figure S65 for CL images with analytical spot locations). Three analyses of xenocrystic cores of two zircon grains yielded $^{206}Pb/^{207}Pb$ dates in excess of 1700 Ma, while all other analyses (N = 10) of magmatic zones in 9 zircon grains yielded Oligocene $^{206}Pb/^{238}U$ dates. The conventional weighted mean computed using these 10 analyses is 30.70 ± 0.35 (0.45) Ma (95% CI, *MSWD* = 1.16; external uncertainty includes the error in the decay constant for ^{238}U and the age of the standard R33 [43]; Figure 7). Note that the 10 analyses of magmatic zones in the M945-R zircons have very similar $^{232}Th/^{238}U$ ratios with an average value of 0.60. Chondrite-normalized REE data (normalized using the composition of McDonough and Sun [47]; Figure S66), as well as Hf, U, and Th abundances are given in Table S8. All $^{40}Ar/^{39}Ar$ and SHRIMP-RG U-Th-Pb and trace element data are available in Mercer et al. [48].

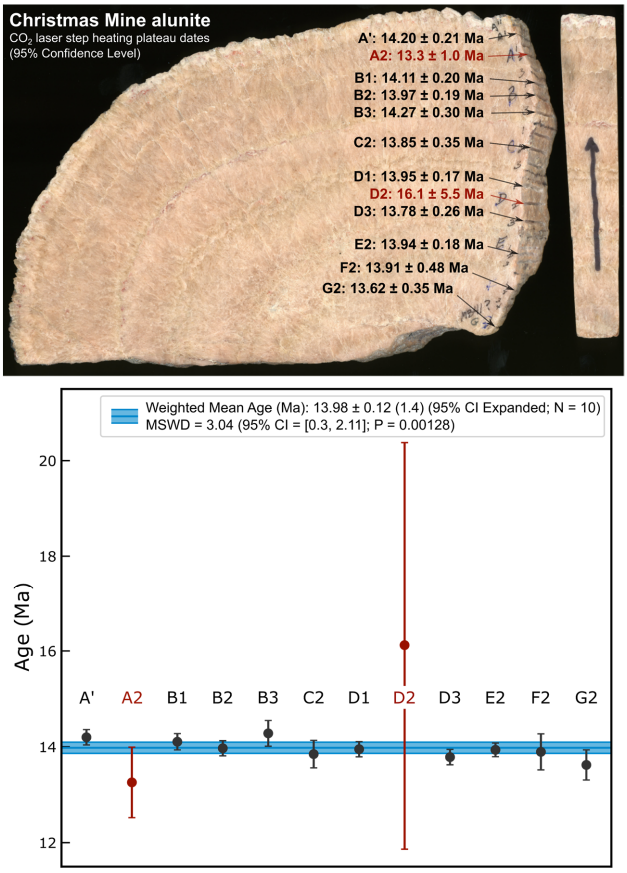

Figure 5. Summary of $^{40}Ar/^{39}Ar$ results for 12 aliquots of 7 bands from a slab of vein alunite from the Christmas mine, sample M341. (See Figures S3–S14 and Table 1 for external uncertainties of the individual plateau dates.) Two aliquots (A2 and D2) were excluded from a weighted mean of the remaining 10 aliquots that yielded a date of 13.98 ± 0.12 (1.1) Ma (95% CI). The uncertainty has been expanded by $\sqrt{MSWD}$ because the value of the $MSWD$ (3.04) falls outside of the 95% CI of the $MSWD$ ([0.3, 2.11]) for (N – 1) = 9 degrees of freedom. Uncertainties are all plotted at 2σ.

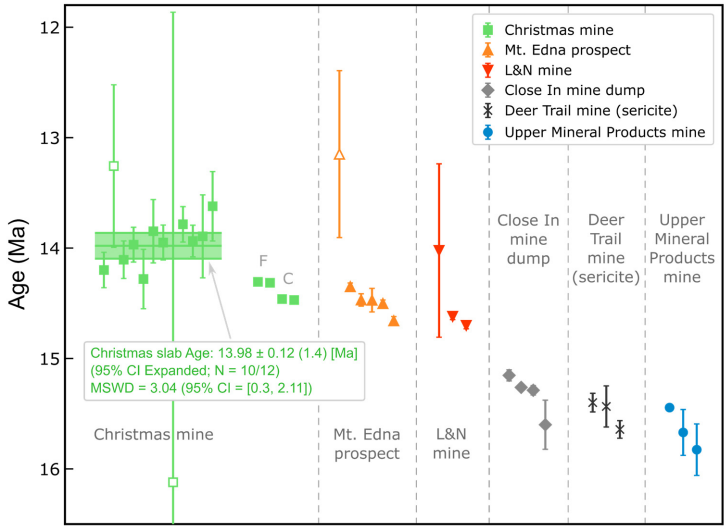

Figure 6. Summary of $^{40}Ar/^{39}Ar$ plateau and weighted mean dates for all magmatic-steam alunite samples, as well as a sample of sericite from the Deer Trail mine. The weighted mean of 10 aliquots of the banded slab from the Christmas mine is shown by the green bar with 95% confidence bounds (see Figure 5; external uncertainty in parentheses). Uncertainties are all plotted at 2σ.

Table 3. SHRIMP-RG U/Pb data for zircon grains separated from M945-R, a sample of a rhyolitic quartz-porphyry dike at the upper Mineral Products mine, Alunite Ridge, Marysvale, Utah. Uncertainties for $^{206}Pb/^{238}U$ and $^{207}Pb/^{206}Pb$ ages are rounded to two significant figures, and the corresponding dates are rounded to the same decimal place.

										^{207}Pb Corrected		^{204}Pb Corrected										
Spot Name	Spot Location	Common ^{206}Pb (%)	U ppm	Th ppm	^{232}Th/^{238}U	Total ^{238}U/^{206}Pb	% 1σ Error	Total ^{207}Pb/^{206}Pb	% 1σ Error	^{206}Pb/^{238}U Age (Ma)	1σ Error (Ma)	^{238}U/^{206}Pb	% 1σ Error	^{207}Pb/^{206}Pb	% 1σ Error	Radiogenic ^{207}Pb/^{235}U	% 1σ Error	Radiogenic ^{206}Pb/^{238}U	% 1σ Error	r	^{207}Pb/^{206}Pb Age (Ma)	1σ Error (Ma)	Discordance (%)
M945-1C	magmatic center	0.07	335	179	0.55	208.17	1.50	0.0472	6.82	30.87	0.48	210.32	1.66	0.0390	17.25	0.0256	17.33	0.00476	1.66	0.10			
M945-2T	magmatic mantle	1.03	199	142	0.74	211.13	1.90	0.0548	7.98	30.15	0.60	215.51	2.32	0.0385	30.62	0.0247	30.71	0.00464	2.32	0.08			
M945-3T	magmatic mantle	−0.22	351	177	0.52	211.35	1.45	0.0449	6.75	30.50	0.46	212.82	1.51	0.0393	11.91	0.0255	12.01	0.00470	1.51	0.13			
M945-4	magmatic mantle	0.61	307	135	0.46	210.43	1.55	0.0514	6.76	30.38	0.49	213.30	1.85	0.0407	22.06	0.0263	22.13	0.00469	1.85	0.08			
M945-5	magmatic mantle	0.31	398	223	0.58	205.85	1.33	0.0491	5.93	31.14	0.43	207.16	1.38	0.0441	10.00	0.0294	10.09	0.00483	1.38	0.14			
M945-6.1	magmatic center	0.09	275	210	0.79	206.84	1.65	0.0474	7.36	31.06	0.53	209.87	1.90	0.0358	23.66	0.0235	23.73	0.00477	1.90	0.08			
M945-6.2	magmatic mantle	1.06	383	202	0.54	213.37	1.40	0.0550	5.99	29.82	0.43	214.83	1.46	0.0496	9.67	0.0319	9.77	0.00466	1.46	0.15			
M945-7.1	unzoned core	1.44	220	65	0.31	3.8236	0.56	0.1049	0.76	1478.4	8.1	3.8249	0.56	0.1046	0.78	3.7715	0.96	0.26143	0.56	0.58	1708	14	14.1
M945-7.2	unzoned core	0.92	106	34	0.33	3.6067	0.79	0.1048	1.07	1565	12	3.6092	0.79	0.1042	1.11	3.9802	1.36	0.27705	0.79	0.58	1700	20	7.8
M945-7.3	magmatic mantle	−0.40	430	249	0.60	209.54	1.29	0.0434	6.13	30.82	0.41	217.31	1.87	0.0140	84.51	0.0089	84.54	0.00461	1.87	0.02			
M945-8.1	light-CL core	3.33	163	62	0.39	5.0548	0.77	0.1053	1.02	1128.1	8.5	5.0576	0.77	0.1049	1.06	2.8584	1.32	0.19771	0.77	0.59	1712	20	47.2
M945-8.2	magmatic mantle	0.43	179	101	0.58	207.18	2.04	0.0500	8.83	30.91	0.65	212.89	2.65	0.0283	52.56	0.0184	52.63	0.00470	2.65	0.05			
M945-9	magmatic mantle	16.92	283	173	0.63	168.61	1.40	0.1805	3.75	31.69	0.56	201.07	3.90	0.0540	56.64	0.0372	56.77	0.00500	3.90	0.07			

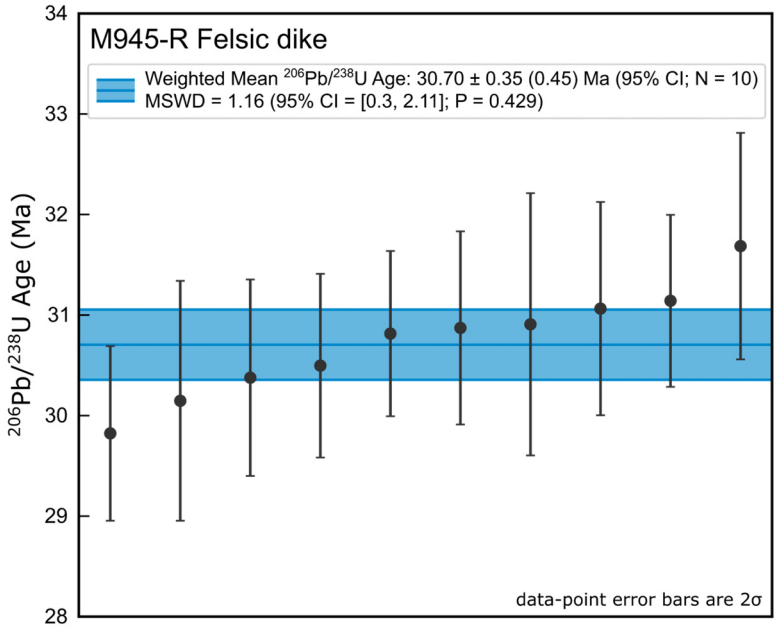

Figure 7. Weighted mean of 10 SHRIMP-RG $^{206}Pb/^{238}U$ results for magmatic zones of 9 zircons from sample M945-R. External age uncertainties (in parentheses following the internal uncertainties) include the uncertainty in the age of the standard R33 [43].

5. Discussion

5.1. Timing of Felsic Intrusive Activity Relative to the Formation of the Three Creeks Tuff Member of the Bullion Canyon Volcanics

The quartz-rhyolite porphyry dike and the Three Creeks Tuff Member of the broadly 34–22 Ma Bullion Canyon Volcanics on each side of the alunite vein at upper Mineral Products have been altered to quartz, alunite, and pyrite. Our weighted mean zircon $^{206}Pb/^{238}U$ date of 30.70 ± 0.35 (0.45) Ma for the rhyolite dike demonstrates that it was emplaced during the period of Oligocene calc-alkaline volcanism (Figure 7). The 31–28 Ma "felsite" dikes that have been dated by geologists from MAG Silver Corp. [30] are clearly also part of this period of Oligocene calc-alkaline igneous activity. However, there are conflicting dates published for the Three Creeks Tuff Member of the Bullion Canyon Volcanics. Plagioclase and biotite K/Ar dates published by Caskey and Shuey [24] and Steven et al. [15] (recalculated to use parameters consistent with those used here) range from 32.16 ± 0.70 (0.82) Ma to 26.95 ± 1.10 (1.16) Ma, and zircon fission track dates are 27.4 ± 1.3 and 27.0 ± 1.2 Ma [15,25]. Steven et al. [15] considered the older dates to be unreliable since they are older than the underlying Wah Wah Springs Tuff Member of the Needles Range Group, which they considered to be 28.9 Ma, and because the 27.5 ± 0.4 Ma date originally reported by Caskey and Shuey [24] was for a sample at the base of the Three Creeks Tuff Member. Rowley et al. [25] concurred with this assessment and considered a 27.1 Ma average of the younger $^{40}Ar/^{39}Ar$ and zircon fission track dates to be the best estimate for the age of the Three Creeks Tuff Member.

However, Steven et al. [15] and Rowley et al. [25] may not have accounted for differences in decay and isotopic abundance values, which can be significant (e.g., [38]). When recalculated using the parameters of Steven et al. [15], the date for the sample of the Three Creeks Tuff Member published by Caskey and Shuey [24] becomes 28.22 ± 0.41 (0.84) Ma, and when recalculated using our preferred parameters it becomes 28.27 ± 0.41 (0.84) Ma (Table S1). Both recalculated values are older than the ca. 27 Ma age interpreted by Steven et al. [15] and Rowley et al. [25] as the likely age of the Three Creeks Tuff Member, but are younger than our weighted mean zircon $^{206}Pb/^{238}U$ date for the rhyolite dike. While the 30.06 ± 0.10 (0.16) Ma weighted mean of 11 plateau dates reported more recently by Best et al. [26] (Table S2) for samples of the Wah Wah Springs Tuff Member is permissive

of an older age for the overlying Three Creeks Tuff Member, it is also younger than our $^{206}Pb/^{238}U$ date for the rhyolite dike (though it overlaps with the young end of the distribution of SHRIMP-RG spot dates). Furthermore, a recalculated date of 31.45 ± 0.31 (0.87) Ma (Table S1) was reported by Caskey and Shuey [24] for the Wah Wah Springs Tuff Member, so the 28.9 Ma value that was used to dismiss older dates for the Three Creeks Tuff Member may be questionable. Regardless, since the rhyolite dike we sampled from the upper Mineral Products mine cuts what has been mapped as the Three Creeks Tuff Member (Figure 3) [31], it must be older than ca. 30.7 Ma or the rocks exposed at Alunite Ridge may in fact be older and miscorrelated with younger rocks in the region. We recognize our data set is limited to one dike, but the 31–28 Ma dates reported by geologists from MAG Silver Corp also indicate that older dikes are present cutting the Bullion Canyon Volcanics. Additional work is needed to refine geologic and geochronologic constraints for volcanic and intrusive rocks in the Alunite Ridge and Deer Trail Mountain area.

5.2. Timing and Spatial Distribution of Miocene Hydrothermal Activity at Alunite Ridge and Deer Trail Mountain

Magmatic-steam alunite from Alunite Ridge and Deer Trail Mountain near Marysvale preserves a record of at least two periods of magmatic degassing from ca. 15.7–15.1 Ma and from ca. 14.7–13.8 Ma (Figures 6 and 8). The older episode of magmatic-steam alunite formation is recorded at the Close In and Mineral Products localities, which are located to the east and southeast, respectively, of the other localities (Figures 3 and 8; recall that the Close In deposit is in a landslide that originated from Deer Trail Mountain). The 15.643 ± 0.087 Ma to 15.400 ± 0.090 Ma sericite dates for sample M992 from the Deer Trail mine provide additional evidence for this older period of hydrothermal activity and consequent alteration of the country rocks. In addition, the ca. 16–15.5 Ma dates published by Waltenberg [27] and Ren and Vasconcelos [28] from diffusion experiments on multiple irradiated aliquots of one sample of vein-type alunite support the timing of this initial episode of hydrothermal activity. Unfortunately, it is unclear precisely from where the sample these authors analyzed was collected, though its age suggests it was from the Mineral Products or Close In mines at Alunite Ridge. Steven et al. [15] did not recognize the earlier ca. 15.7–15.1 Ma pulse of magmatic degassing as the two samples they analyzed from the Mineral Products mine yielded younger dates of ca. 14.3–13.8 Ma. However, given the approximately 20 m width of this alunite vein, it is not surprising that both magmatic episodes are recorded in this single vein system.

The younger episode of magmatic degassing is clearly recorded at the Christmas and L&N mines and the Mt. Edna prospect. Given that 10 of the 12 aliquots (all M341 aliquots excluding A2 and D2) from seven alunite bands in the banded slab from the Christmas mine yielded a weighted mean of 13.98 ± 0.12 Ma (Figure 5), we interpret the bands to have completely formed within a period of ca. 250 ka (based on the 95% CI of the weighted mean). While the older apparent age of aliquot D2 of the banded slab (M341) can be explained by very low $^{40}Ar^*$ yields, the younger apparent ages of aliquot M341 A2 and sample 003-05 from the Mt. Edna prospect are more enigmatic. Closure temperatures reported for both supergene and hypogene alunite, assuming a range of cooling rates from 5–100 °C/Ma, are consistently higher ($\gtrsim$200 °C) [28,49,50] than the 90–180 °C temperatures expected for the formation of magmatic-steam alunite [12,22]. Diffusion modeling also indicates that prolonged heating at the lower steam-heated temperatures would require excessive durations to cause any significant Ar loss (e.g., 100 Ma if alunite is held at 100 °C) [28]. In addition, the preservation within banded alunite of multicomponent gas signatures with contributions from crustal and meteoric sources (e.g., [21,51]) precludes significant thermal overprinting.

Therefore, there is no obvious natural mechanism for thermally driven Ar loss at Alunite Ridge, implying the younger apparent ages of M341 A2 and 003-05 either (1) reflect a later pulse of hydrothermal activity, (2) are due to Ar loss resulting from physical alteration/defects in the mineral structures of the analyzed aliquots of alunite, or (3) are

simple analytical artefacts. Since the band from which M341 A2 was derived is situated between two other bands with ca. 14 Ma dates (Figure 5), and given the large uncertainties associated with both M341 A2 and 003-05, we consider these dates to be unreliable (for either of reasons 2 or 3 above) and find it most likely that hydrothermal activity ceased by 14 Ma or shortly thereafter (within a few hundred ka). Furthermore, given the retentivity of alunite in the steam-heated environment and lack of evidence for subsequent thermal overprinting at Alunite Ridge, individual cm-scale bands of alunite are likely to accurately record their formation age. Thus, the relatively short (likely $\lesssim$250 ka) period over which the seven alunite bands developed in the slab sampled from the Christmas mine is consistent with a short recurrence interval of $\lesssim$36 ka for magmatic steam exhalation. Additional high-precision $^{40}Ar/^{39}Ar$ geochronology of individual bands in a more extensive sample of banded alunite (e.g., from the 20 m-wide vein at the upper Mineral Products mine), combined with robust statistical analysis (such as the methods employed by Morgan et al. [52]), could further refine constraints on the duration of each period of magmatic degassing at Alunite Ridge.

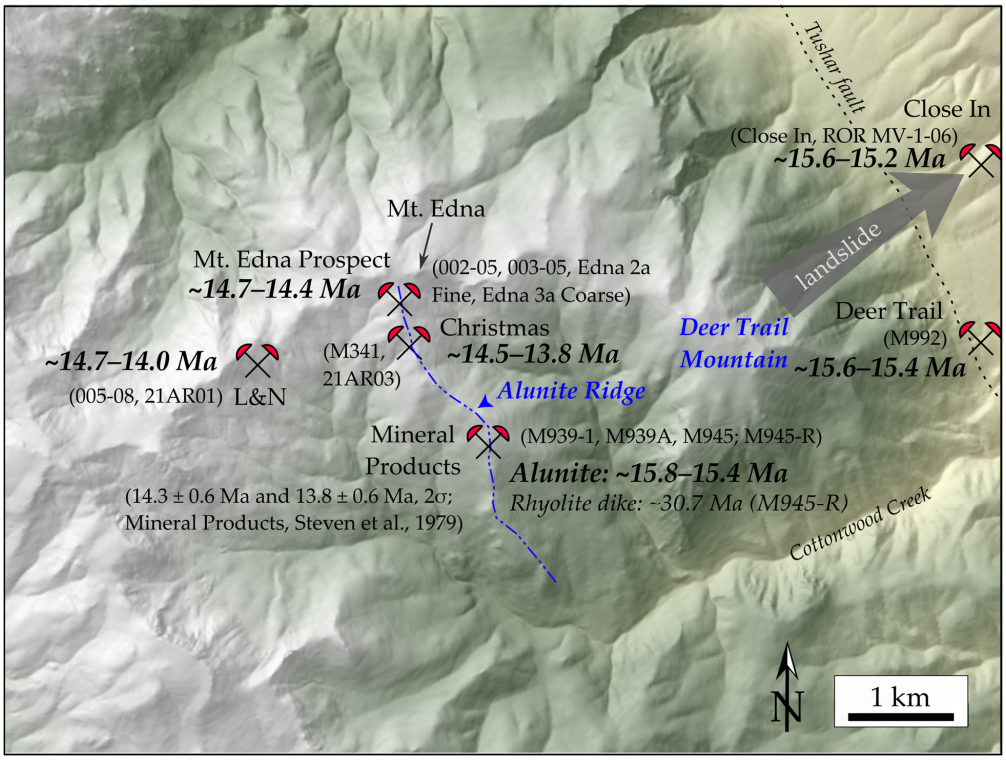

Figure 8. Summary of the ranges of $^{40}Ar/^{39}Ar$ dates for magmatic-steam alunite and sericite from the mines and prospects sampled here. Two K/Ar dates published by Steven et al. [15] for samples of magmatic-steam alunite from the upper Mineral Products mine are listed as well (with internal uncertainties only; see Section 2.1 and Table S1 for external uncertainties). The location shown for the Deer Trail mine marks the portal; the workings extend ca. 3200 m to the west beneath Deer Trail Mountain [14].

5.3. Relation to Regional Tectonic and Igneous Activity

The geologic model in which a concealed composite pluton was emplaced with one stock beneath Deer Trail Mountain and another beneath Alunite Ridge is supported by multiple lines of geologic and geochemical evidence [13,14,16,53]. Our $^{40}Ar/^{39}Ar$ results provide additional high-precision geochronologic support for this model. The 15.7–15.1 Ma dates for vein-type alunite and sericite alteration from the eastern Close In, Mineral Products, and Deer Trail mines may define an initial phase of magmatic degassing associated with initial intrusion of a porphyry stock beneath Deer Trail Mountain. This episode of activity may also be associated with the CRD deposit at the Deer Trail mine (e.g., [13,14]).

Then, some 0.5–1.5 Ma later, a second phase of intrusion occurred beneath Alunite Ridge to form a second porphyry stock, and consequent hydrothermal activity produced the alunite veins at the Mineral Products, Christmas, L&N, and Mt. Edna mines over several hundred ka. These Miocene intrusions likely overprinted an Oligocene rhyolitic intrusion that was the source for the rhyolite dikes we observed at the Mineral Products, Christmas, and Bradburn mines (Figure 9).

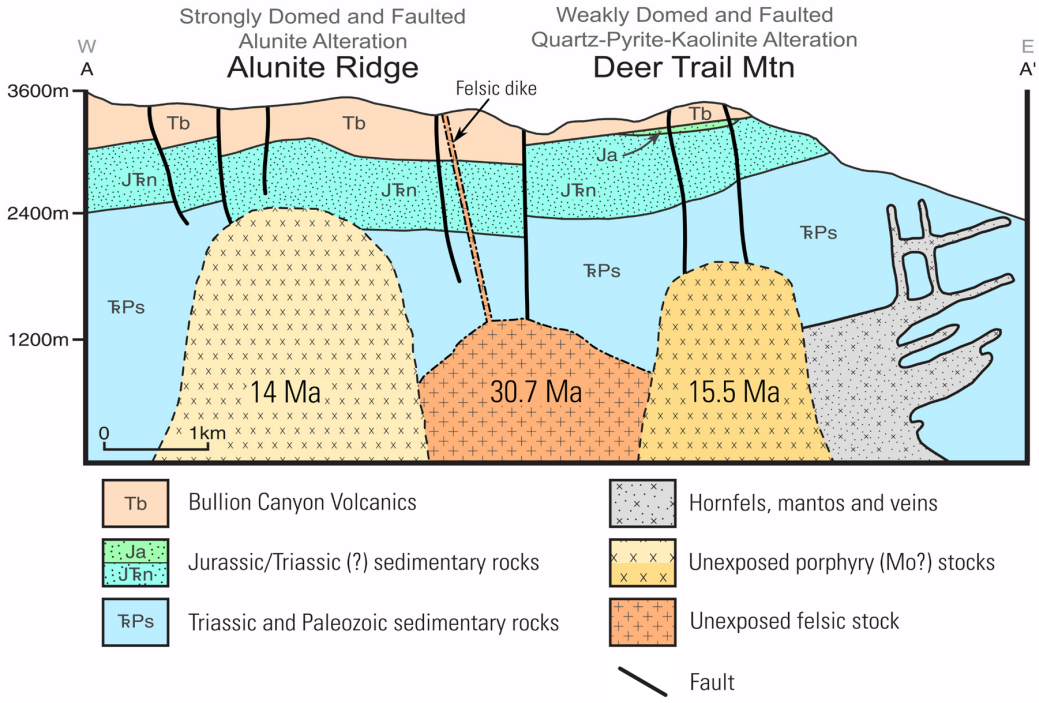

Figure 9. Schematic cross section showing the inferred position of multiple intrusive stocks beneath Alunite Ridge and Deer Trail Mountain (modified after Beaty et al. [14]). See Figure 3 for the location of the cross section. An Oligocene rhyolitic stock is inferred to be the source of rhyolitic quartz-porphyry dikes like the one dated at the upper Mineral Products mine and others at the Bradburn and Christmas mines. The two Miocene stocks (likely similar to those in Climax-type porphyry Mo systems) are inferred to be the sources for the magmatic volatiles that episodically produced magmatic-steam alunite during two periods at ca. 15.7–15.1 Ma and ca. 14.7–13.8 Ma. These periods of hydrothermal activity may have produced (or overprinted) the carbonate replacement deposit at the Deer Trail mine.

The timing of Miocene intrusive and hydrothermal activity at Deer Trail Mountain and Alunite Ridge is consistent with the migration of bimodal basalt-rhyolite magmatism across the Marysvale volcanic field (Figure 2) [18], and with broader patterns of Miocene bimodal igneous activity in southwestern Utah (e.g., [54]). Furthermore, the change around 22 Ma from calc-alkaline to bimodal basalt-rhyolite magmatic activity in the Marysvale volcanic field is consistent with the more regional compositional shifts within the Basin and Range Province that occurred during the late Oligocene to Miocene [55–59]. These shifts are thought to reflect the coincident evolution from subduction of the Farallon plate to subduction of a transform boundary of the East Pacific Rise along the west coast of California during the Miocene (e.g., [26,55–59]). Prior to this shift in composition, the dominantly calc-alkaline magmatism that swept from north to south in the northern Basin and Range Province and from south to north in the southern Basin and Range Province was a consequence of the progressive removal of the Farallon plate that exposed the chilled and hydrated continental lithosphere to hot upwelling asthenosphere (e.g., [57–61]).

Within this tectonic context, the last calc-alkaline events to occur in the Marysvale-Deer Trail area were the eruption of the Monroe Peak caldera and emplacement of the Central

intrusion at ca. 23 Ma (Figure 2), and the eruption of the Delano Peak Tuff Member of the Bullion Canyon Volcanics ca. 22 Ma [15,16]. Bimodal igneous activity then promptly followed as asthenospheric mantle drove melting in the hydrated and thinned continental lithosphere, migrating from the northeast towards the southwest in the Marysvale area (Figure 2). As this activity terminated near present day Alunite Ridge, felsic magmas were generated in part through partial melting associated with intrusion of subcontinental lithospheric mantle-derived basalts into the crust. These felsic magmas episodically released supercritical fluids that rapidly ascended, variably entraining crustal volatiles and meteoric water, and finally precipitated magmatic-steam alunite [51].

5.4. Implications for Mineral Exploration

Published geologic, geochemical, and geochronologic data (e.g., [13,14]) and our $^{40}Ar/^{39}Ar$ results for magmatic-steam alunite and sericite from the mines and prospects at Alunite Ridge and Deer Trail Mountain suggest that the dominant period of hydrothermal activity was in the Miocene as a result of the intrusion of two porphyry stocks. However, our data do not preclude the possibility that Miocene intrusive and hydrothermal activity overprinted a previous Oligocene hydrothermal system associated with the emplacement of the rhyolite dikes in the Bullion Canyon Volcanics. Additional work is needed to conclusively determine the age, or ages, of the CRD in the Deer Trail mine.

While most porphyry Cu systems are located in continental and oceanic arcs and associated with subduction-related igneous rocks (e.g., Dilles and John [1] and references therein), the inferred stocks beneath Alunite Ridge and Deer Trail were emplaced in an extensional "postsubduction" tectonic setting that produced Climax-type porphyry Mo systems (e.g., [1,13,16]). From our results, the durations of individual periods of magmatic and associated hydrothermal activity (with episodic discharge of magmatic steam) at Alunite Ridge and Deer Trail Mountain are comparable to those observed in other Climax-type systems for which high-precision geochronology data are available. For example, at the Questa porphyry Mo deposit (~400 kt MoS_2), the total duration of mineralizing magmatism was ca. 770 ka with Mo mineralization lasting $\lesssim$500 ka [9,10]. The durations of mineralizing magmatism at the Pine Grove (~450 kt MoS_2) and Victorio (~250 kt MoS_2) porphyry Mo deposits are <2 Ma (e.g., [62,63]). In addition, the cumulative duration of the two periods of Miocene magmatic/hydrothermal activity at Alunite Ridge and Deer Trail Mountain is approximately 1.5 Ma. This is comparable to the durations of intrusive and hydrothermal activity at the Los Pelambres (ca. 2 Ma, 36 Mt Cu) and El Teniente (ca. 1.6–2 Ma, 95 Mt Cu) porphyry Cu deposits (see Figure S11 of Chelle-Michou et al. [5]).

Since the duration of intrusive activity exerts a first-order control on the endowment of porphyry Cu deposits [5], this might be cautiously viewed as an indicator that the concealed (and potentially relatively long-lived) Climax-type porphyry system below Alunite Ridge and Deer Trail Mountain may not be barren. At the least, the episodic release of magmatic S over the course of ~1.5 Ma of felsic magmatism makes the Alunite Ridge/Deer Trail Mountain area an appealing exploration target for porphyry-style sulfide mineralization. However, we caution that this is speculative, as the method of Chelle-Michou and coworkers [5] was developed for well-exposed and well-characterized porphyry Cu deposits in subduction-related tectonic settings. Furthermore, the link between the durations of magmatic/hydrothermal activity and the endowment of Climax-type porphyry Mo deposits is not yet well-understood [62], and mineralization may be limited by the availability of external S (e.g., from mafic magmas; [64]) during the period when rapidly cooling (i.e., short-lived) felsic porphyries are releasing Mo-rich fluids (e.g., [9]). Regardless, $^{40}Ar/^{39}Ar$ geochronology to determine the age and duration of magmatic-steam alunite formation is clearly a valuable tool for identifying concealed porphyry systems in either subduction-related or extensional tectonic settings.

Supplementary Materials: The following supporting information can be downloaded at: https://www.mdpi.com/article/10.3390/min12121533/s1, Supplementary Figures S1–S66: All $^{40}Ar/^{39}Ar$ release spectra, inverse isochrons, and probability density plots, as well as zircon CL images, and SHRIMP trace element figures; Table S1: Published K/Ar data for igneous rocks and vein and replacement alunite in the Marysvale area, Utah; Table S2: Published $^{40}Ar/^{39}Ar$ data for vein alunite from the Marysvale area, Utah; Table S3: Latitude and longitude of samples; Table S4: Irradiation chronologies; Table S5: Nucleogenic production ratios; Table S6: Summary of $^{40}Ar/^{39}Ar$ inverse isochron dates for samples of magmatic-steam alunite from Alunite Ridge and Deer Trail Mountain, Marysvale, Utah; Table S7: $^{40}Ar/^{39}Ar$ data for magmatic-steam and replacement alunite from Alunite Ridge and Deer Trail Mountain, Marysvale, Utah; Table S8: SHRIMP-RG trace element data for M945-R zircons.

Author Contributions: Conceptualization, R.O.R. and G.P.L.; data curation, C.M.M.; formal analysis, C.M.M. and W.R.P.; investigation, C.M.M., M.A.C. and W.R.P.; methodology, C.M.M., M.A.C. and W.R.P.; project administration, M.A.C., A.H.H., R.O.R. and G.P.L.; resources, C.M.M., M.A.C., A.H.H., R.O.R. and G.P.L.; validation, C.M.M., M.A.C. and W.R.P.; visualization, C.M.M. and W.R.P.; writing—original draft, C.M.M., M.A.C., A.H.H. and W.R.P.; writing—review and editing, C.M.M., M.A.C., A.H.H., W.R.P., R.O.R. and G.P.L. All authors have read and agreed to the published version of the manuscript.

Funding: This research was funded by the U.S. Geological Survey Mineral Resources Program.

Data Availability Statement: The data presented in this study are available in the Supplementary Material, and in an accompanying USGS data release by Mercer et al. [48] (https://doi.org/10.5066/P9IF4UZP).

Acknowledgments: We are grateful to Charles Cunningham (deceased) for his many contributions to understanding the geology of Alunite Ridge and its surroundings and George Breit for providing sericite separates of sample M992. We also thank Jay Thompson, Leah Morgan, and Phillip Verplanck for assistance in the field, and Neil Griffis for field assistance as well as helpful discussions about the SHRIMP and $^{40}Ar/^{39}Ar$ data. We thank Joshua Rosera, Alejandra Angulo, and three anonymous reviewers for their detailed and constructive comments that improved this manuscript. Any use of trade, firm, or product names is for descriptive purposes only and does not imply endorsement by the U.S. Government.

Conflicts of Interest: The authors declare no conflict of interest.

References

1. Dilles, J.H.; John, D.A. Porphyry and Epithermal Mineral Deposits. In *Encyclopedia of Geology*; Alderton, D., Elias, S.A., Eds.; Academic Press: Cambridge, MA, USA, 2021; pp. 847–866.
2. Wang, L.; Qin, K.-Z.; Song, G.-X.; Li, G.-M. A Review of Intermediate Sulfidation Epithermal Deposits and Subclassification. *Ore Geol. Rev.* **2019**, *107*, 434–456. [CrossRef]
3. Kirkham, R.V. Intermineral Intrusions and Their Bearing on the Origin of Porphyry Copper and Molybdenum Deposits. *Econ. Geol.* **1971**, *66*, 1244–1249. [CrossRef]
4. Cathles, L.M.; Erendi, A.H.J.; Barrie, T. How Long Can a Hydrothermal System Be Sustained by a Single Intrusive Event? *Econ. Geol.* **1997**, *92*, 766–771. [CrossRef]
5. Chelle-Michou, C.; Rottier, B.; Caricchi, L.; Simpson, G. Tempo of Magma Degassing and the Genesis of Porphyry Copper Deposits. *Sci. Rep.* **2016**, *7*, 40566. [CrossRef] [PubMed]
6. von Quadt, A.; Erni, M.; Martinek, K.; Moll, M.; Peytcheva, I.; Heinrich, C.A. Zircon Crystallization and the Lifetimes of Ore-Forming Magmatic-Hydrothermal Systems. *Geology* **2011**, *39*, 731–734. [CrossRef]
7. Catchpole, H.; Kouzmanov, K.; Bendezú, A.; Ovtcharova, M.; Spikings, R.; Stein, H.; Fontboté, L. Timing of Porphyry (Cu-Mo) and Base Metal (Zn-Pb-Ag-Cu) Mineralisation in a Magmatic-Hydrothermal System—Morococha District, Peru. *Miner. Depos.* **2015**, *50*, 895–922. [CrossRef]
8. Spencer, E.T.; Wilkinson, J.J.; Creaser, R.A.; Seguel, J. The Distribution and Timing of Molybdenite Mineralization at the El Teniente Cu-Mo Porphyry Deposit, Chile. *Econ. Geol.* **2015**, *110*, 387–421. [CrossRef]
9. Rosera, J.M.; Coleman, D.S.; Stein, H.J. Re-evaluating Genetic Models for Porphyry Mo Mineralization at Questa, New Mexico: Implications for Ore Deposition Following Silicic Ignimbrite Eruption. *Geochem. Geophys. Geosyst.* **2013**, *14*, 787–805. [CrossRef]
10. Gaynor, S.P.; Rosera, J.M.; Coleman, D.S. Intrusive History of the Oligocene Questa Porphyry Molybdenum Deposit, New Mexico. *Geosphere* **2019**, *15*, 548–575. [CrossRef]

11. Chiaradia, M. Gold Endowments of Porphyry Deposits Controlled by Precipitation Efficiency. *Nat. Commun.* **2020**, *11*, 248. [CrossRef]
12. Rye, R.O. A Review of the Stable-Isotope Geochemistry of Sulfate Minerals in Selected Igneous Environments and Related Hydrothermal Systems. *Chem. Geol.* **2005**, *215*, 5–36. [CrossRef]
13. Cunningham, C.G.; Rye, R.O.; Steven, T.A.; Mehnert, H.H. Origins and Exploration Significance of Replacement and Vein-Type Alunite Deposits in the Marysvale Volcanic Field, West Central Utah. *Econ. Geol.* **1984**, *79*, 50–71. [CrossRef]
14. Beaty, D.W.; Cunningham, C.G.; Rye, R.O.; Steven, T.A.; Gonzalez-Urien, E. Geology and Geochemistry of the Deer Trail Pb-Zn-Ag-Au-Cu Manto Deposits, Marysvale District, West-Central Utah. *Econ. Geol.* **1986**, *81*, 1932–1952. [CrossRef]
15. Steven, T.A.; Cunningham, C.G.; Naeser, C.W.; Mehnert, H.H. *Revised Stratigraphy and Radiometric Ages of Volcanic Rocks and Mineral Deposits in the Marysvale Area, West-Central Utah*; Geological Survey Bulletin 1469; U.S. Geological Survey: Liston, VA, USA, 1979; 40p.
16. Cunningham, C.G.; Rasmussen, J.D.; Steven, T.A.; Rye, R.O.; Rowley, P.D.; Romberger, S.B.; Selverstone, J. Hydrothermal Uranium Deposits Containing Molybdenum and Fluorite in the Marysvale Volcanic Field, West-Central Utah. *Miner. Depos.* **1998**, *33*, 477–494. [CrossRef]
17. Rowley, P.D.; Cunningham, C.G.; Anderson, J.J.; Steven, T.A.; Workman, J.B.; Snee, L.W. Geology and Mineral Resources Of The Marysvale Volcanic Field, Southwestern Utah. In Proceedings of the Rocky Mountain Section Annual Meeting, Cedar City, UT, USA, 7–9 May 2002; Geological Society of America: Boulder, CO, USA, 2002.
18. Cunningham, C.G.; Ludwig, K.R.; Naeser, C.W.; Weiland, E.K.; Mehnert, H.H.; Steven, T.A.; Rasmussen, J.D. Geochronology of Hydrothermal Uranium Deposits and Associated Igneous Rocks in the Eastern Source Area of the Mount Belknap Volcanics, Marysvale, Utah. *Econ. Geol.* **1982**, *77*, 453–463. [CrossRef]
19. Callaghan, E. *Mineral Resource Potential of Piute County, Utah and Adjoining Area*; Utah Geological and Mineralogical Survey Bulletin 102; Utah Geological and Mineralogical Survey: Salt Lake City, UT, USA, 1973.
20. Cunningham, C.G.; Rye, R.O.; Rockwell, B.W.; Kunk, M.J.; Councell, T.B. Supergene Destruction of a Hydrothermal Replacement Alunite Deposit at Big Rock Candy Mountain, Utah: Mineralogy, Spectroscopic Remote Sensing, Stable-Isotope, and Argon-Age Evidences. *Chem. Geol.* **2005**, *215*, 317–337. [CrossRef]
21. Landis, G.P.; Rye, R.O. Characterization of Gas Chemistry and Noble-Gas Isotope Ratios of Inclusion Fluids in Magmatic-Hydrothermal and Magmatic-Steam Alunite. *Chem. Geol.* **2005**, *215*, 155–184. [CrossRef]
22. Rye, R.O.; Bethke, P.M.; Wasserman, M.D. The Stable Isotope Geochemistry of Acid Sulfate Alteration. *Econ. Geol.* **1992**, *87*, 225–262. [CrossRef]
23. Bassett, W.A.; Kerr, P.F.; Schaeffer, O.A.; Stoenner, R.W. Potassium-Argon Dating of the Late Tertiary Volcanic Rocks and Mineralization of Marysvale, Utah. *GSA Bull.* **1963**, *74*, 213–220. [CrossRef]
24. Caskey, C.F.; Shuey, R.T. Mid-Tertiary Volcanic Stratigraphy, Sevier-Cove Fort Area, Central Utah. *Utah Geol.* **1975**, *2*, 17–25. [CrossRef]
25. Rowley, P.D.; Mehnert, H.H.; Naeser, C.W.; Snee, L.W.; Cunningham, C.G.; Steven, T.A.; Anderson, J.J.; Sable, E.G.; Anderson, R.E. *Isotopic Ages and Stratigraphy of Cenozoic Rocks of the Marysvale Volcanic Field and Adjacent Areas, West-Central Utah*; U.S. Geological Survey Bulletin 2071; U.S. Geological Survey: Liston, VA, USA, 1994; p. 35.
26. Best, M.G.; Christiansen, E.H.; Deino, A.L.; Gromme, S.; Hart, G.L.; Tingey, D.G. The 36–18 Ma Indian Peak–Caliente Ignimbrite Field and Calderas, Southeastern Great Basin, USA: Multicyclic Super-Eruptions. *Geosphere* **2013**, *9*, 864–950. [CrossRef]
27. Waltenberg, K.M. Mineral Physics and Crystal Chemistry of Minerals Suitable for Weathering Geochronology: Implications to $^{40}Ar/^{39}Ar$ and (U-Th)/He Geochronology. Ph.D. Thesis, The University of Queensland, Brisbane, Australia, 2012.
28. Ren, Z.; Vasconcelos, P.M. Argon Diffusion in Hypogene and Supergene Alunites: Implications to Geochronology and Thermochronometry on Earth and Mars. *Geochim. Cosmochim. Acta* **2019**, *262*, 166–187. [CrossRef]
29. MAG Silver Corp. MAG Silver Reports Successful Phase 1 Deer Trail Drilling Results. MAG Silver Corporate News Reports, 2021. Available online: https://magsilver.com/news/mag-silver-reports-successful-phase-1-deer-trail-drilling-results/ (accessed on 24 August 2022).
30. MAG Silver Corp. Deer Trail Technical Presentation, MAG Silver Corporate Videos, 2020. Available online: https://magsilver.com/investors/corporate-videos/ (accessed on 24 August 2022).
31. Rowley, P.D.; Cunningham, C.G.; Steven, T.A.; Workman, J.B.; Anderson, J.J.; Theissen, K.M. *Geologic Map of the Central Marysvale Volcanic Field, Southwestern Utah*; U.S. Geological Survey: Denver, CO, USA, 2002; IMAP 2645-A. [CrossRef]
32. Dalrymple, G.B.; Alexander, E.C., Jr.; Lanphere, M.A.; Kraker, G.P. *Irradiation of Samples for $^{40}Ar/^{39}Ar$ Dating Using the Geological Survey TRIGA Reactor*; Geological Survey Professional Paper 1176; U.S. Geological Survey: Washington, DC, USA, 1981; 55p.
33. Turrin, B.D.; Swisher, C.C.; Deino, A.L. Mass Discrimination Monitoring and Intercalibration of Dual Collectors in Noble Gas Mass Spectrometer Systems. *Geochem. Geophys. Geosyst.* **2010**, *11*, Q0AA09. [CrossRef]
34. Lee, J.-Y.; Marti, K.; Severinghaus, J.P.; Kawamura, K.; Yoo, H.-S.; Lee, J.B.; Kim, J.S. A Redetermination of the Isotopic Abundances of Atmospheric Ar. *Geochim. Cosmochim. Acta* **2006**, *70*, 4507–4512. [CrossRef]
35. Fleck, R.J.; Sutter, J.F.; Elliot, D.H. Interpretation of Discordant $^{40}Ar/^{39}Ar$ Age-Spectra of Mesozoic Tholeiites from Antarctica. *Geochim. Cosmochim. Acta* **1977**, *41*, 15–32. [CrossRef]
36. Kuiper, K.F.; Deino, A.; Hilgen, F.J.; Krijgsman, W.; Renne, P.R.; Wijbrans, J.R. Synchronizing Rock Clocks of Earth History. *Science* **2008**, *320*, 500–504. [CrossRef]

37. Min, K.; Mundil, R.; Renne, P.R.; Ludwig, K.R. A Test for Systematic Errors in $^{40}Ar/^{39}Ar$ Geochronology through Comparison with U/Pb Analysis of a 1.1-Ga Rhyolite. *Geochim. Cosmochim. Acta* **2000**, *64*, 73–98. [CrossRef]
38. Mercer, C.M.; Hodges, K.V. ArAR—A Software Tool to Promote the Robust Comparison of K–Ar and $^{40}Ar/^{39}Ar$ Dates Published Using Different Decay, Isotopic, and Monitor-Age Parameters. *Chem. Geol.* **2016**, *440*, 148–163. [CrossRef]
39. Pearson, R.K. *Exploring Data in Engineering, the Sciences, and Medicine*; Oxford University Press: New York, NY, USA, 2011; 770p.
40. Mahon, K.I. The New York Regression: Application of an Improved Statistical Method to Geochemistry. *Int. Geol. Rev.* **1996**, *38*, 293–303. [CrossRef]
41. York, D.; Evensen, N.M.; Martínez, M.L.; Delgado, J.D.B. Unified Equations for the Slope, Intercept, and Standard Errors of the Best Straight Line. *Am. J. Phys.* **2004**, *72*, 367–375. [CrossRef]
42. Wendt, I.; Carl, C. The Statistical Distribution of the Mean Squared Weighted Deviation. *Chem. Geol. Isot. Geosci. Sect.* **1991**, *86*, 275–285. [CrossRef]
43. Black, L.P.; Kamo, S.L.; Allen, C.M.; Davis, D.W.; Aleinikoff, J.N.; Valley, J.W.; Mundil, R.; Campbell, I.H.; Korsch, R.J.; Williams, I.S.; et al. Improved $^{206}Pb/^{238}U$ Microprobe Geochronology by the Monitoring of a Trace-Element-Related Matrix Effect: SHRIMP, ID–TIMS, ELA–ICP–MS and Oxygen Isotope Documentation for a Series of Zircon Standards. *Chem. Geol.* **2004**, *205*, 115–140. [CrossRef]
44. Williams, I.S. U-Th-Pb Geochronology by Ion Microprobe; Not Just Ages but Histories. In *Applications of Microanalytical Techniques to Understanding Mineralizing Processes*; McKibben, M.A., Shanks, W.C., Ridley, W.I., Eds.; Society of Economic Geologists Reviews in Economic Geology: Littleton, CO, USA, 1998; Volume 7, pp. 1–35.
45. Ireland, T.R.; Williams, I.S. Considerations in Zircon Geochronology by SIMS. *Rev. Mineral. Geochem.* **2003**, *53*, 215–241. [CrossRef]
46. Ludwig, K.R. *SQUID 1.02, A Users Manual*; Berkeley Geochronology Center Special Publication 2; Berkeley Geochronology Center: Berkeley, CA, USA, 2001; 19p.
47. McDonough, W.F.; Sun, S. The Composition of the Earth. *Chem. Geol.* **1995**, *120*, 223–253. [CrossRef]
48. Mercer, C.M.; Cosca, M.A.; Premo, W.R. Argon and SHRIMP-RG Data for Magmatic Steam Alunite, Sericite, and Zircon from Alunite Ridge and Deer Trail Mountain, Marysvale, Utah. U.S. *Geol. Surv. Data Release* **2022**. [CrossRef]
49. Love, D.A.; Clark, A.H.; Hodgson, C.J.; Mortensen, J.K.; Archibald, D.A.; Farrar, E. The Timing of Adularia-Sericite-Type Mineralization and Alunite-Kaolinite-Type Alteration, Mount Skukum Epithermal Gold Deposit, Yukon Territory, Canada; ^{40}Ar-^{39}Ar and U-Pb Geochronology. *Econ. Geol.* **1998**, *93*, 437–462. [CrossRef]
50. Landis, G.P.; Snee, L.W.; Juliani, C. Evaluation of Argon Ages and Integrity of Fluid-Inclusion Compositions: Stepwise Noble Gas Heating Experiments on 1.87 Ga Alunite from Tapajós Province, Brazil. *Chem. Geol.* **2005**, *215*, 127–153. [CrossRef]
51. Landis, G.P.; Rye, R.O. Fluid Inclusion Active and Noble Gases in Coarse-Banded Alunite Veins at Alunite Ridge, Marysvale, Utah, and Implications for Crust-Mantle Magmatic Volatile Evolution [abs]. *Geol. Soc. Am. Abstr. Programs* **2009**, *41*, 525.
52. Morgan, L.E.; Johnstone, S.A.; Gilmer, A.K.; Cosca, M.A.; Thompson, R.A. A Supervolcano and Its Sidekicks: A 100 Ka Eruptive Chronology of the Fish Canyon Tuff and Associated Units of the La Garita Magmatic System, Colorado, USA. *Geology* **2019**, *47*, 453–456. [CrossRef]
53. Cunningham, C.G.; Steven, T.A. *Geologic Map of the Deer Trail Mountain-Alunite Ridge Mining Area, West-Central Utah*; U.S. Geological Survey Miscellaneous Investigation Series; U.S. Geological Survey: Liston, VA, USA, 1979; Map I-1230, Scale 1:24,000. [CrossRef]
54. Best, M.G.; McKee, E.H.; Damon, P.E. Space-Time-Composition Patterns of Late Cenozoic Mafic Volcanism, Southwestern Utah and Adjoining Areas. *Am. J. Sci.* **1980**, *280*, 1035–1050. [CrossRef]
55. Lipman, P.W.; Prostka, H.J.; Christiansen, R.L. Evolving Subduction Zones in the Western United States, as Interpreted from Igneous Rocks. *Science* **1971**, *174*, 821–825. [CrossRef] [PubMed]
56. Dickinson, W.R. The Basin and Range Province as a Composite Extensional Domain. *Int. Geol. Rev.* **2002**, *44*, 1–38. [CrossRef]
57. Best, M.G.; Christiansen, E.H.; de Silva, S.; Lipman, P.W. Slab-Rollback Ignimbrite Flareups in the Southern Great Basin and Other Cenozoic American Arcs: A Distinct Style of Arc Volcanism. *Geosphere* **2016**, *12*, 1097–1135. [CrossRef]
58. McQuarrie, N.; Oskin, M. Palinspastic Restoration of NAVDat and Implications for the Origin of Magmatism in Southwestern North America. *J. Geophys. Res. Solid Earth* **2010**, *115*, B10401. [CrossRef]
59. Glazner, A.F. Cenozoic Magmatism and Plate Tectonics in Western North America: Have We Got It Wrong? In *In the Footsteps of Warren B. Hamilton: New Ideas in Earth Science*; Foulger, G.R., Hamilton, L.C., Jurdy, D.M., Stein, C.A., Howard, K.A., Stein, S., Eds.; Geological Society of America Special Paper 553; The Geological Society of America: Boulder, CO, USA, 2022; pp. 95–108.
60. Humphreys, E.; Hessler, E.; Dueker, K.; Farmer, G.L.; Erslev, E.; Atwater, T. How Laramide-Age Hydration of North American Lithosphere by the Farallon Slab Controlled Subsequent Activity in the Western United States. *Int. Geol. Rev.* **2003**, *45*, 575–595. [CrossRef]
61. Humphreys, E. Relation of Flat Subduction to Magmatism and Deformation in the Western United States. In *Backbone of the Americas: Shallow Subduction, Plateau Uplift, and Ridge and Terrane Collision*; Kay, S.M., Ramos, V.A., Dickinson, W.R., Eds.; The Geological Society of America: Boulder, CO, USA, 2009; Volume 204, pp. 85–98, ISBN 9780813712048.
62. Rosera, J.M.; Gaynor, S.P.; Frazer, R.E. The Magmatic Duration of Climax-type Porphyry Mo Systems. In Proceedings of the SEG 2022 Meeting: Minerals for Our Future, Denver, CO, USA, 27–30 August 2022; Abstract P5.07.

63. Keith, J.D.; Shanks, W.C.; Archibald, D.A.; Farrar, E. Volcanic and Intrusive History of the Pine Grove Porphyry Molybdenum System, Southwestern Utah. *Econ. Geol.* **1986**, *81*, 553–577. [CrossRef]
64. Mercer, C.N.; Hofstra, A.H.; Todorov, T.I.; Roberge, J.; Burgisser, A.; Adams, D.T.; Cosca, M. Pre-Eruptive Conditions of the Hideaway Park Topaz Rhyolite: Insights into Metal Source and Evolution of Magma Parental to the Henderson Porphyry Molybdenum Deposit, Colorado. *J. Petrol.* **2015**, *56*, 645–679. [CrossRef]